

1 Nitrite Cycling in the Primary Nitrite Maxima of the Eastern 2 Tropical North Pacific

3 Formatted

4 Nicole M. Travis¹, Colette L. Kelly¹, Margaret R. Mulholland², Karen L. Casciotti¹

5 Formatted: Font color: Text 1

6 ¹ Earth System Science, Stanford University, Stanford CA, 94305, USA

7 ² Department of Ocean, Earth and Atmospheric Science, Old Dominion University, Norfolk VA, 23529, USA

8 Correspondence to: Nicole M. Travis (ntravis@stanford.edu)

9 Deleted: depth

10 Deleted: maxima

11 Deleted: the

12 Deleted: maxima

13 Deleted: fewer

14 Deleted: rate processes active in

15 Deleted: cycling

16 Deleted: depth

17 Deleted: concentration of the maxima.

18 Deleted: a major producer

19 Deleted: (Gruber, 2008).

20 Deleted: , e.g.,

48 where primary production is confined, but abundant in waters below the euphotic zone. Other inorganic fixed N species,
49 e.g., nitrite and ammonium, are present in smaller quantities, and their production and consumption are tightly coupled
50 in the marine environment. In the upper ocean, the nitracline demarcates a spatial transition where nitrate, nitrite and
51 ammonium may all be available to microbes simultaneously. In particular, the primary nitrite maximum (PNM) is a
52 ubiquitous feature of the upper ocean. In the Pacific Ocean, the median nitrite concentration across PNM features is
53 237 nM (GLODAP), although concentrations as high as 2.8 μ M have been reported (Brandhorst, 1958; Carlucci et al.,
54 1970; Dore and Karl, 1996; Wada and Hattori, 1972; GLODAP, V2). In addition, nitrite can be present throughout
55 the entire surface water column (Lomas and Lipschultz, 2006; Zakem et al., 2018). The accumulation of nitrite at the
56 PNM occurs at a depth horizon where dynamic N cycling occurs, and it can appear and disappear within the span of
57 only 25 meters. The PNM location generally coincides not only with the top of the nitracline, but also with the depth
58 of the oxycline, the depth of the chlorophyll maximum, and just below or coincident with an ammonium maximum
59 near the base of the euphotic zone (Dore and Karl, 1996; Herblant and Voituriez, 1979; Holligan et al., 1984; Kiefer
60 et al., 1976; Zafiriou et al., 1992; Zakem et al., 2018). The consistent strong spatial relationships between nitrite,
61 nitrate, and chlorophyll concentrations hint at a relationship between these environmental parameters and nitrite
62 production, but does not provide a clear mechanism.

Deleted: but

Deleted: , where nitrite often accumulates to concentrations near 300 nM, although concentrations as high as 2.8 μ M have been reported (Brandhorst, 1958; Carlucci et al., 1970; Dore and Karl, 1996; GLODAP, V2; Wada and Hattori, 1972). While in some cases

Deleted:), nitrite concentrations are below detection in most of the ocean because nitrite is an intermediate formed during oxidation of reduced N (NH_4^+ , DON) (Zehr and Kudela, 2011; Zehr and Ward, 2002).

Deleted: and both

Deleted: bacterial and archaeal nitrifiers

Deleted: making it difficult

Deleted: determine

Deleted: to produce the nitrite concentrations observed,

Deleted: differentially

Deleted: and ultimately what factors influence the magnitude and depth of the PNM

Deleted:

Deleted:

Formatted: No underline, Underline color: Auto

104 the lack of strong light inhibition of ammonia oxidation in some studies (Horak et al., 2018; Merbt et al., 2012; Smith
105 et al., 2014). Additionally, nitrification rates are substrate-dependent and constrained to places and times when
106 ammonia and nitrite are both available (Martens-Habbena et al., 2009). Nitrite is also taken up by phytoplankton but
107 this process is thought to be light dependent (Lomas and Glibert, 2000; Mulholland and Lomas, 2008). Nitrite release
108 from phytoplankton is also well documented in culture studies (Al-Qutob et al., 2002; Collos, 1998), but it is still
109 unclear whether nitrite release occurs during incomplete nitrate reduction under low light conditions when energy for
110 its complete assimilation is limited, under fluctuating high light conditions as a photoprotective mechanism, or as a
111 stress response to high light levels (Collos, 1982; Kiefer et al., 1976; Lomas and Glibert, 1999, 2000; Wada and Hattori,
112 1971).

113 Accumulation of nitrite occurs when the rate of its production exceeds that of its loss via consumption, or diffusion.
114 Thus, the presence of the PNM is an indicator of conditions where production and consumption of nitrite are, or have
115 recently been, imbalanced (Wada and Hattori, 1971). The accumulation of nitrite in the PNM may provide valuable
116 insight into the balance of relative rates of microbial nitrite cycling in the upper ocean, as it indicates a zone where
117 biologically mediated processes are not in balance and may be experiencing differential inhibition or limitation. Rarely
118 are the four major microbial processes related to PNM formation (ammonia oxidation, nitrite oxidation, nitrate
119 reduction and nitrite uptake) measured simultaneously in the field. The few paired rate measurements that exist tend
120 to show that ammonia oxidation rates exceed nitrite oxidation rates in the PNM, suggesting nitrite oxidation is the rate
121 limiting step in the reaction pair and a potential mechanism for nitrite accumulation (Beman et al., 2013; Schaefer and
122 Hollibaugh, 2017; Füssel et al., 2012; Peng et al., 2015; Santoro et al., 2013; Ward et al., 1982). However, the lack of
123 paired measurements focused on the sharp PNM boundaries limits our understanding of the coupling between the two
124 steps of nitrification or other processes affecting nitrite accumulation across these depths. Higher resolution paired
125 measurements will allow us to investigate how environmental gradients create vertical zonation in the relative rates of
126 nitrite-cycling processes that lead to nitrite accumulation within narrow depth horizons. Previous investigations of the
127 PNM have typically focused on nitrifier communities or phytoplankton communities separately, although it is
128 understood that the niches of these communities overlap, and that both may contribute to nitrite accumulation. The
129 studies that have measured both phytoplankton and nitrifier processes (Mackey et al., 2011; Santoro et al., 2013; Wan
130 et al., 2018; Ward, 2005) support the idea that physiological constraints and competitive interactions between these
131 groups drive resource use and nitrite accumulation (Smith et al., 2014; Wan et al., 2021; Zakem et al., 2018).

132 Understanding the controls on rates of co-occurring nitrite cycling processes will help clarify the distributions of
133 microbial activity and how relative rates of these processes may change due to future environmental perturbations.
134 For example, understanding the controls on and patterns of nitrification in the surface ocean is critical for
135 understanding new production, as estimates suggest more than 30% of oceanic primary production is supported by
136 nitrate supplied by nitrification in the euphotic zone (Santoro et al., 2010; Ward et al., 1989; Yool et al., 2007). In
137 addition, the relative contributions of nitrification and phytoplankton activity to the formation of the PNM may also
138 be important for understanding the potential for nitrous oxide formation in the surface ocean (Burlacot et al., 2020;
139 Kelly et al., 2021; Plouviez et al., 2019; Santoro et al., 2011).

Deleted: .

Deleted: net

Moved down [1]: ; Füssel et al., 2012; Peng et al., 2015; Santoro et al., 2013; Ward et al., 1982).

Deleted: A few studies have measured both steps of nitrification concurrently near the ETNP (Beman et al., 2013

Deleted:

Moved (insertion) [1]

Deleted:).

Deleted: /uncoupling

149 To investigate the relative contributions of nitrification and phytoplankton processes to net accumulation of nitrite at
150 the PNM feature, we measured rates of four microbially-mediated nitrite cycling processes (ammonia oxidation, nitrite
151 oxidation, nitrate reduction and nitrite uptake) in vertical profiles through the PNM. We analyzed spatial and regional
152 variations in environmental conditions and water column features associated with the PNM, as well as the rates of
153 nitrite production and consumption.

Deleted: In the oligotrophic Eastern Tropical North Pacific (ETNP), the PNM occurs as a sharp peak located at the top of the nitracline and within the waning slope of the primary chlorophyll maximum. The PNM also sits above a secondary nitrite maximum (SNM) that occurs within the oxygen deficient waters below.

Formatted: Indent: Left: 0", First line: 0"

154 2 Methods

155 2.1 Hydrography and nutrient analyses

156 This study is based on data collected from four cruises to the Eastern Tropical North Pacific Ocean (ETNP) between
157 April 2016 and June 2018 (RB1603 – *R/V Ronald Brown*, April 2016; SKQ201617s – *R/V Sikuliaq*, December 2016;
158 SR1805 – *R/V Sally Ride*, April 2018; and FK180624 – *R/V Falkor*, June 2018; Figure 1). The ETNP hosts one of the
159 largest oceanic oxygen deficient zones (ODZs) and is a region of active nitrogen cycling. Oxygen concentrations
160 decline precipitously from saturated surface water concentrations to nanomolar levels across the oxycline in much of
161 the study area (Cline and Richards, 1972), with oxygen deficient waters beginning as shallow as 15 m at some coastal
162 stations. This study focused on nitrite cycling in the upper water column near the PNM, and all rate data were collected
163 in oxygenated waters in or above the oxycline.

164 Fifty-three stations were occupied during these cruises, and hydrographic observations of temperature, salinity, and
165 oxygen were made using a CTD package (RB1603 – Sea-Bird SBE 11+ CTD, SKQ201617s/SR1805/FK180624 –
166 Sea-Bird SBE 911+ CTD). Fluorescence and photosynthetically active radiation (PAR) measurements were measured
167 at a subset of stations (RB1603 – LiCor Biospherical Photosynthetically Active Radiation Sensor/SeaPoint
168 Chlorophyll Fluorometer). Discrete water samples were collected from Niskin bottles mounted to the CTD rosette to
169 measure dissolved inorganic N concentrations. Nitrite and ammonium concentration measurements were typically
170 made immediately onboard the ship, while samples for nitrate concentration measurements were 0.22 μ m filtered and
171 frozen in 60-ml HDPE bottles for analysis at a shore-based laboratory. During the 2016 cruise, a pump profiling system
172 (PPS; as described in Codispoti et al., 1991) was also deployed with a separate CTD package (Seabird SBE19+,
173 WetStar Fluorometer) at all 16 stations.

Formatted: No underline, Underline color: Auto

174 For all cruises, nitrite concentrations were measured colorimetrically with a detection limit of ~200 nM (Strickland
175 and Parsons, 1972). Briefly, five ml of sample water from each Niskin bottle was reacted with 200 μ l each of
176 sulfanilamide and N-(1-NAPHTHYL)ethylenediamine reagents, and absorbance at 543 nm was measured after a 10
177 min reaction time and converted to concentration using a standard curve, with an overall precision of $\pm 0.006 \mu$ M.
178 Ammonium concentrations were measured shipboard using a fluorometric method after derivatization with ortho-
179 phthalaldehyde (OPA) reagent (Holmes et al., 1999). Samples and standards were reacted with OPA for ~8 hours at
180 4°C in the dark before measurement. In 2016, samples for nitrate plus nitrite were collected from discrete depths using
181 Niskin bottles mounted to a CTD rosette and analyzed shipboard using an Astoria Pacific autoanalyzer according to
182 the manufacturer's specifications using standard colorimetric methods (Strickland and Parsons, 1972). In 2017, nitrate

Formatted: Font: Times New Roman

189 plus nitrite samples were analyzed using standard colorimetric methods on a Technicon Autoanalyzer at the University
190 of Washington. In 2018, nitrate plus nitrite was measured after Cd reduction using a WestCo SmartChem 200 Discrete
191 Analyzer at Stanford University, with an overall precision of $\pm 0.6 \mu\text{M}$, and detection limit of 85 nM (Miller et al 1998,
192 Rajacovic 2008). Nitrate concentrations were calculated by subtracting nitrite from the concentration of nitrate plus
193 nitrite for all cruises. During the 2016 cruise (RB1603), cast water from the PPS was pumped directly through a Fast
194 Repetition Rate Fluorometer (FRRF) for chlorophyll *a* fluorescence measurements and then to an Alpkem Astoria-
195 Pacific rapid-flow analysis system for near-continuous profiles of nitrate, nitrite, and ammonium concentrations at one
196 measurement per second and binned to every meter (Holmes et al., 1999; Sakamoto et al., 1990; Strickland and Parsons,
197 1972).

198 Water column profiles were analyzed to determine station-specific water column features (Table 1). The depth of the
199 top of the nitracline (Z_{nit}) was identified as the depth at which nitrate concentration increased by 1 μM compared to a
200 reference depth of 20 m (Corne et al., 2021). In addition, the standard nitracline depth (Z_{mnit}) was identified as where
201 the nitrate gradient was steepest. Similarly, the top of the oxycline (Z_{oxy}) was identified as the depth at which oxygen
202 concentration decreased by 5 μM relative to the concentration at a depth of 20 m. The standard oxycline depth (Z_{mox})
203 was where the oxygen gradient was steepest. Other station-specific water column features included the depth and
204 concentration of the nitrite maximum (m and μM , respectively), the depth and concentration of the chlorophyll
205 maximum (m and mg m^{-3} , respectively), the depth and concentration of the ammonium maximum (m and nM,
206 respectively), and the depth at which 1% of the surface photosynthetically active radiance (PAR) was present (m).
207 Concentrations/characteristics of these variables at the depth of the nitrite maximum were also calculated (e.g., nitrate
208 concentration ($\text{NO}_2^-_{\text{pm}}$), chlorophyll concentration (Chl_{pm}), ammonium concentration ($\text{NH}_4^+_{\text{pm}}$), oxygen
209 concentration (O_2_{pm}), temperature (T_{pm}), density (D_{pm}), percent of surface PAR (PAR_{pm})). The Brunt-Väisälä
210 frequency (BV_{pm}) was calculated at the PNM nitrite maximum ($\pm 8 \text{ m}$) using the equation $N = \sqrt{\frac{g}{\rho} * \frac{dp}{dz}}$, where g is
211 the acceleration due to gravity (m s^{-2}), z is depth (m) and ρ is density (kg m^{-3}). Depth-integrated concentrations of
212 nitrate, nitrite, and ammonium ($\mu\text{mol N m}^{-2}$) were calculated for the euphotic zone (upper 120 m), capturing the
213 entirety of the PNM feature.

214 ▲
215 Table 1. Water Column Feature Acronyms, Definitions and Units

Symbol	Definition	Unit
PNM	Primary nitrite maximum, whole feature	—
Chl_{max}	Concentration of the deep chlorophyll maximum	mg m^{-3}
$\text{NH}_4^+_{\text{max}}$	Concentration of the ammonium maximum	nM
$\text{NO}_2^-_{\text{max}}$	Concentration of the PNM nitrite maximum	μM
Z_{chl}	Depth of the deep chlorophyll maximum	m
$Z_{\text{NH}_4^+}$	Depth of the ammonium maximum	m
$Z_{\text{NO}_2^-}$	Depth of the PNM nitrite maximum	m

Deleted: .
Formatted: Font: Times New Roman
Deleted: pump profiling system (PPS)

Deleted: .
Deleted: the inflection point between the nitrate-depleted surface waters and an increase in
Deleted: of
Deleted: surface
Deleted: inflection point between oxygen-replete surface waters, using a reference depth of 20 m, and a decrease in
Deleted: of
Deleted: identified include
Deleted:)
Deleted: 1%
Deleted: level
Deleted: specifically
Deleted: $\text{NO}_3^-_{\text{pm}}$
Deleted: $\text{NH}_4^+_{\text{pm}}$
Deleted:), oxygen concentration (O_{pm}).
Deleted: $\text{NO}_2^-_{\text{pm}}$

Deleted: $N = \sqrt{\frac{g}{\rho} * \frac{dp}{dz}}$,
Formatted: Font: 9 pt, Bold
Formatted: Indent: Left: 0", First line: 0"
Formatted Table
Formatted: Font: 10 pt, Subscript
Formatted: Font: 10 pt
Formatted: Font: 10 pt, Superscript
Deleted: NH_4^{max}
Formatted: Font: 10 pt
Deleted: NO_2^{max}
Formatted: Font: 10 pt
Deleted: Z_{nh}
Formatted: Font: 10 pt
Deleted: Z_{no2}
Formatted: Font: 10 pt

Z_{nit}	Depth of top of the nitracline	m
Z_{minit}	Depth of steepest gradient in nitracline	m
Z_{oxy}	Depth of the top of the oxycline	m
Z_{moxy}	Depth of steepest gradient in oxycline	m
Z_{PAR}	Depth of 1% surface PAR	m
Chl_{PNM}	Chlorophyll concentration at the PNM peak	mg m^{-3}
$\text{NH}_4^+_{\text{PNM}}$	Ammonium concentration at the PNM peak	nM
$\text{NO}_3^-_{\text{PNM}}$	Nitrate concentration at the PNM peak	μM
T_{PNM}	Temperature at the PNM peak	C
D_{PNM}	Density at the PNM peak	kg m^{-3}
PAR_{PNM}	Percent of surface PAR at the PNM peak	%
O_2_{PNM}	Oxygen concentration at the PNM peak	μM
BV_{PNM}	Brunt Väisälä Frequency at the PNM peak	s^{-1}
$\text{NH}_4^+_{\text{Int}}$	Depth integrated ammonium over upper 120 m	nmol N m^{-2}
$\text{NO}_2^-_{\text{Int}}$	Depth integrated nitrite over upper 120 m	$\mu\text{mol N m}^{-2}$
$\text{NO}_3^-_{\text{Int}}$	Depth integrated nitrate over upper 120 m	$\mu\text{mol N m}^{-2}$
Chl_{Int}	Depth integrated chlorophyll over upper 120 m	mg m^{-2}

243

244

2.2 Nitrite cycling rates

245 Rates of ammonia oxidation, nitrite oxidation, nitrate reduction and nitrite uptake were measured at 12 of the 53
 246 stations occupied over 4 cruises from 2016-2018 (Fig. 1a), **including** five stations from 2016, two stations in 2017,
 247 and five stations in 2018. At each of these stations during a pre-dawn cast, 3-4 depths near the PNM were sampled
 248 based on real-time CTD fluorescence data during the downcast, targeting depths both within the chlorophyll maximum
 249 and on the upslope and downslope of its peak (Table S1). When available, nitrite profiles from previous casts were
 250 consulted to guide sampling based on the location of the PNM within the chlorophyll maximum.

251 From each depth, six clear 500-ml **polycarbonate (PC)** Nalgene bottles were triple-rinsed and filled directly from the
 252 Niskin bottle for light incubations. Additionally, six 500-ml or 1-L amber **high-density polyethylene (HDPE)** Nalgene
 253 bottles were triple-rinsed and filled for paired dark incubations. One of three ^{15}N -labeled nitrogen substrates (K^{15}NO_3
 254 enriched at 99.5 atm%, $\text{Na}^{15}\text{NO}_2$ enriched at 98.8 atm% or $^{15}\text{NH}_4\text{Cl}$ enriched at 99.5 atm%) was added to duplicate
 255 bottles to achieve enrichments of 200 nM ^{15}N . **High tracer enrichment in samples with low ambient concentrations**
 256 **may lead to enhancement of rates, which are best characterized as potential rates; care must be taken when interpreting**
 257 **results.** After gentle mixing, a 60 ml subsample was **syringe**-filtered (0.22 μm pore size, **Sterivex**) to determine initial
 258 concentration and ^{15}N enrichment of the substrate pool. Approximately 10 ml was used for shipboard measurement of
 259 the initial concentrations of total nitrite or ammonium (ambient concentration plus ^{15}N -labeled DIN addition). The
 260 **remaining** 50 ml was frozen at -20 °C in a 60-ml HDPE bottle for measurement of total nitrate concentration and
 261 isotopic enrichment **in a shore-based laboratory.**

Formatted	[1]
Formatted: Font: 10 pt, Subscript	
Formatted	[2]
Formatted	[3]
Deleted: Z_{PAR}	
Formatted: Font: 10 pt	
Formatted	[4]
Formatted: Font: 10 pt, Superscript	
Deleted: NH_4pnm	
Formatted: Font: 10 pt	
Deleted: NO_3pnm	
Formatted: Font: 10 pt	
Deleted: O_2pnm	
Formatted: Font: 10 pt	
Formatted	[5]
Formatted	[6]
Formatted: Font: 10 pt, Superscript	
Formatted	[7]
Deleted: Opnm	
Formatted: Font: 10 pt	
Formatted	[8]
Formatted: Font: 10 pt, Superscript	
Deleted: _	
Deleted: 120m	
Formatted: Subscript	
Deleted: _	
Deleted: 120m	
Formatted: Subscript	
Deleted: 120m	
Deleted:);	
Deleted: Rate measurements for microbial nitrite cycling processes were made using ^{15}N -tracer incubation experiments. ...rom each depth, six clear 500-ml HDPE ... [9]	
Deleted: 5atm... atm%, $\text{Na}^{15}\text{NO}_2$ enriched at 98.8atm... atm% or $^{15}\text{NH}_4\text{Cl}$ enriched at 99.5atm ... [10]	
Deleted: Sterivex	
Deleted:) using a syringe	
Deleted: other	

304 Each incubation bottle was placed in a deck-board incubator that approximated the ambient light level from the sample
305 collection depth, achieved using neutral density screening. The percent PAR in the incubators was recorded using a
306 submersible Licor PAR meter or an *in situ* HOBO light and temperature logger (~1%,~4%,~20% surface PAR).
307 Incubators were plumbed with flow-through surface seawater to maintain a consistent water temperature. However,
308 surface water temperatures were often significantly warmer than those at collection depth and could have biased some
309 of the incubation results. Subsamples were collected from each incubation bottle after approximately 8, 16 and 24 hrs.
310 Samples were syringe-filtered (0.22 μ m pore size Sterivex) and frozen in 60-ml HDPE bottles for nutrient and isotope
311 analysis in a shore-based laboratory. At the end of the incubation (24 hr), the remaining ~300 ml of water was filtered
312 onto a pre-combusted (450°C for > 4 h) GF/F (0.7 μ m) filter; the filter was folded and placed into a cryovial and stored
313 at -80 °C for later analysis of particulate $\delta^{15}\text{N}$ at the University of Hawaii Isotope Lab. All seawater samples were
314 stored frozen until the time of isotopic analysis. Incubation bottles were acid washed and re-used for experiments
315 using the same ^{15}N substrate.

316 2.3 Isotope analysis and rate calculations

317 For estimates of ammonia oxidation, nitrite oxidation and nitrate reduction rates, samples collected from each
318 timepoint were analyzed for ^{15}N enrichment of the respective product pool (Table 2). For each sample, the product
319 was converted to nitrous oxide either by bacterial (*P. aureofaciens*) conversion using the denitrifier method (McIlvin
320 and Casciotti, 2011; Sigman et al., 2001) or chemical conversion using the azide method (McIlvin and Altabet, 2005).
321 Isotopic analysis via the denitrifier method was used for measurement of $^{15}\text{NO}_x$ (ie. $^{15}\text{NO}_3^- + ^{15}\text{NO}_2$) in ammonia
322 oxidation and nitrite oxidation experiments. Measurements of nitrite oxidation required pre-treatment of samples to
323 remove any remaining $^{15}\text{N-NO}_2$ prior to analysis of $\delta^{15}\text{N-NO}_3$ (Granger and Sigman, 2009). Briefly, 10 ml of each
324 sample was treated with 100 μ l of 4% sulfamic acid in 10% hydrochloric acid for 15 min, after which the pH was
325 neutralized using 85 μ l of 2M sodium hydroxide before proceeding with denitrifier method. Samples were prepared
326 in volumes targeting 20 nmoles nitrate. The azide method was used to prepare nitrite produced from nitrate reduction
327 experiments for isotopic analysis (McIlvin and Altabet, 2005). Nitrite was converted to nitrous oxide by incubating
328 for ~30 min with a 2M sodium azide solution in 20% acetic acid. The reaction was neutralized with 6M sodium
329 hydroxide prior to isotope analysis. Since nitrite product concentrations were low (<2 μM), a significant portion of
330 the nitrite in the samples was newly created from ^{15}N -labeled nitrate, thus carrier nitrite (5-10 nmoles) of known
331 isotope value was added to dilute the ^{15}N enrichment and increase overall concentration of nitrite in the samples before
332 isotopic analysis. Samples were analyzed in volumes targeting 10 nmoles of nitrite.

333 The isotopic composition of the nitrous oxide produced from each sample was measured in the Casciotti Laboratory
334 at Stanford University using an isotope ratio mass spectrometer (Thermo-Finnigan Delta^{PLUS} XP) fitted with a custom
335 purge-and-trap gas purification and concentration system (McIlvin and Casciotti, 2011). Each set of 9 samples was
336 bracketed with international reference materials to correct for instrument drift and sample size, and to calibrate isotope
337 values. USGS32, USGS34, and USGS35 (Böhlke et al., 2003) were used to calibrate nitrate isotope analyses, and
338 RSIL-N23, N7373 and N10219 (Casciotti et al., 2007) were used to calibrate nitrite isotope analyses. For nitrate

Deleted: in situ

Deleted: temperatures

Deleted: Sterivex

Deleted: filtrate

Deleted: analysis

Formatted: Indent: Left: 0", First line: 0"

Deleted: in

Deleted: for each process

Deleted:

Deleted: plus nitrite.

Deleted: 215

Deleted: 216

Formatted: Font: Calibri

Deleted: 217

Deleted: 218

Deleted: front219 end

Deleted: 220

Formatted: Font: Calibri

Deleted: 221

Deleted: 222

Formatted: Font: Calibri

Deleted: 223

349 reduction samples, additional mass balance corrections were made to correct for the addition of nitrite carrier to the
 350 product pool before calculation of rates. The denitrifier method for natural abundance nitrate isotope analyses typically
 351 has a precision of better than 0.5‰ for $\delta^{15}\text{N}$ (McIlvin and Casciotti, 2011; Sigman et al., 2001), although standard
 352 deviations are often higher for isotopically enriched samples. Here, the mean analytical precision of $\delta^{15}\text{N-NO}_3$, $\delta^{15}\text{N-}$
 353 NO_3 , $\delta^{15}\text{N-NO}_2$ measurements of ^{15}N -labeled samples were $\pm 4.2\%$, $\pm 4.6\%$ and $\pm 0.7\%$, respectively, corresponding
 354 to mean coefficient of variance (CV%) of 5.3%, 0.56% and 9.7%, respectively (Table 2).

355 **Table 2. Nitrite cycling reactant and product pools as analyzed by isotope rate mass spectrometry.**

Microbial Process	Reactant	Product	Prep Method	Precision(‰)	CV %
Ammonia Oxidation	$^{15}\text{NH}_4\text{Cl}$	$^{15}\text{NO}_3 + ^{15}\text{NO}_2$	Denitrifier	4.2	5.3
Nitrite Oxidation	$\text{Na}^{15}\text{NO}_2$	$^{15}\text{NO}_3$	Sulfamic-treated + Denitrifier	4.6	0.56
Nitrate Reduction	K^{15}NO_3	$^{15}\text{NO}_2$	Azide w/carrier	0.7	9.7

357
 358 Rate calculations were made by tracking the increase in product ^{15}N over the incubation period (Ward, 1985). For
 359 ammonia oxidation the equation is as follows:

$$360 V_{\text{NH}_3} = \frac{\Delta [^{15}\text{NO}_X]_{t_8-t_0}}{af^{15}\text{NH}_3_{t_0} \times \Delta t \times 24} \quad (1)$$

361 where $\Delta [^{15}\text{NO}_X]_{t_8-t_0}$ is the change in product $^{15}\text{NO}_X$ concentration between the start of the incubation and the 8 h
 362 timepoint (nM), $af^{15}\text{NH}_3_{t_0}$ is the atom fraction of $^{15}\text{NH}_3$ substrate available at the start of the incubation period,
 363 and Δt is the change in time (hours). While the initial ^{15}N in the substrate pool was directly measured at time zero
 364 for use in rate calculations, the addition of 200 nM ^{15}N tracer led to variable atom fraction of ^{15}N in the substrate
 365 pool across experiments, which was calculated from ambient and tracer substrate concentrations. Paired dark and
 366 light incubation samples were used to convert hourly rates to daily rates using a simple assumption of a 12 hr
 367 light:12 hr dark daily cycle. The ammonia oxidation rate, V_{NH_3} , is thus reported in units of nM N day⁻¹. A similar
 368 equation was used to calculate nitrite oxidation and nitrate reduction rates, substituting the appropriate substrate and
 369 product species for each process (Table 1). Some dark incubation data were not available for nitrate reduction
 370 measurements in 2016, so those daily rates were calculated using 24 hr light incubated rates and may be
 371 overestimates. The 16 h and 24 h time point samples were analyzed but not used to calculate rates as experiments
 372 showed non-linear trends after 8 hours of incubation due to substrate depletion. Based on a threshold increase in
 373 product $\delta^{15}\text{N}$ compared to the initial product, a theoretical detection limit was calculated to estimate the rate we can
 374 reasonably expect to discern from zero (Santoro et al., 2013). This calculation is sensitive to both the $\delta^{15}\text{N}$ of the
 375 substrate pool, the concentration of the product pool, and the CV% for $\delta^{15}\text{N}$ measurements. The threshold for
 376 detectable change in product $\delta^{15}\text{N}$ was approximated using the maximum CV% for each experiment. For example, if

- Deleted: 224
 Deleted: 225
 Deleted: 226 ...lthough standard deviations are often ... [11]
 Deleted: 229 →
 Formatted ... [12]
 Deleted: after conversion to 230 →nitrous oxide via ... [13]
 Formatted ... [14]
 Deleted:
 Formatted ... [15]
 Formatted ... [16]
 Formatted Table ... [17]
 Deleted: ^{15}N -labeled
 Formatted ... [18]
 Formatted ... [19]
 Moved (insertion) [2]
 Formatted ... [20]
 Formatted ... [21]
 Moved down [3]: Prep Method
 Moved up [2]: Product
 Moved (insertion) [3]
 Formatted ... [22]
 Formatted ... [23]
 Deleted: ^{15}N -labeled
 Deleted: Mean
 Formatted ... [24]
 Formatted ... [25]
 Deleted: 1
 Deleted: Mean
 Formatted ... [27]
 Formatted ... [28]
 Formatted ... [29]
 Formatted ... [30]
 Formatted ... [31]
 Deleted: NH_4Cl
 Formatted ... [32]
 Moved down [4]: Denitrifier
 Formatted ... [33]
 Moved (insertion) [4]
 Formatted ... [34]
 Deleted: $\text{NO}_3^-/\text{NO}_2^-$
 Formatted ... [35]
 Formatted ... [36]
 Formatted ... [37]
 Formatted ... [38]
 Formatted ... [39]
 Moved down [5]: Sulfamic-treated + Denitrifier
 Moved (insertion) [5]
 Deleted: NaNO_2
 Deleted: NO_3^-
 Formatted ... [42]
 Formatted ... [43]
 Formatted ... [45]
 Formatted ... [46]
 Formatted ... [40]
 Formatted ... [41]
 Formatted ... [44]
 Formatted ... [47]
 Formatted ... [48]
 Formatted ... [49]

379 the standard deviation in replicates for a sample with a $\delta^{15}\text{N}$ of 25‰ was ± 0.6 , a CV% of 2.4% was used as the
380 theoretical detectable difference between initial and final ^{15}N enrichment in the product pool. Where available, the
381 maximum CV% for each experimental unit was used to calculate the theoretical limit of detection for each depth
382 (Table S1b). The mean theoretical detection limits for ammonia oxidation, nitrite oxidation and nitrate reduction
383 were 0.5, 6.9, and 0.9 nM day $^{-1}$, respectively. Experimental bottle duplicates were conducted for most rate
384 measurements and those standard deviations are reported with the final rate data (Table S1b).

385 Filters from nitrite uptake rate experiments were dried overnight and packed in tin capsules before shipment to the
386 Biogeochemical Stable Isotope Facility at the University of Hawaii, where samples were analyzed on a Thermo
387 Scientific Delta V Advantage isotope ratio mass spectrometer coupled to a Costech Instruments elemental analyzer.
388 Rate calculations relied on ^{15}N enrichment of the particulate organic nitrogen over the 24 h incubation period as in
389 Dugdale and Goering (1967). Uptake rates were calculated according to Dugdale and Wilkerson (1986) where the
390 initial ^{15}N atom percent fraction of the reactant pool was calculated assuming 0.3663 for the ^{15}N atom percent of the
391 ambient substrate pool and 98.8 atm% $^{15}\text{N-NO}_2^-$ of the isotope tracer addition. Nitrite uptake rates may be
392 underestimated due to dilution of the substrate pool via regeneration over the 24 incubation period, and loss of tracer
393 to unmeasured DON pools (Bronk et al., 1994; Glibert et al., 2019). No correction was made for possible rate
394 enhancement due to tracer addition (Dugdale and Wilkerson, 1986).

395 2.4 Multiple Linear Regression Analysis

396 Multiple linear regression (MLR) models were built to assess the environmental variables that influence the depth and
397 magnitude of the PNM feature in the ETNP. The first set of MLR models ('full' models) used semi-continuous
398 measurements (temperature, density, oxygen, chlorophyll fluorescence, PAR, nitrate, nitrite and ammonium) from
399 CTD/PPS casts collected at 16 stations on the 2016 cruise to predict nitrite concentration. Nitrate, nitrite and
400 ammonium data were natural-log transformed to satisfy normal distribution assumptions of the multiple linear
401 regression analyses. Using the R package *leaps*, the model was optimized using a best-subsets selection of the full
402 variable set to maximize R^2 and minimize root mean squared error for each potential model size using 10-fold cross
403 validation to calculate test error for each sized model (optimization led to selection of 19 variables out of 27 possible
404 explanatory variables – 7 main and 20 single interactions terms) (Miller, 2020). The model size that minimized test
405 error was selected, and a best-subsets selection method was used to determine the optimal variable coefficients. MLR
406 coefficients from the optimized models were then used to predict nitrite concentration for station depth profiles in the
407 ETNP. Three variations on the 'full' model were made using data from: 1) all stations, 2) a subset of coastal stations
408 (6, 7, 8, and 9) and 3) a subset of offshore stations (13, 14, 15 and 16). Subsets of stations were selected as exemplary
409 of the coastal and offshore regimes based on proximity to the coast, concentration of the chlorophyll maxima, and
410 nitracline depths. The selection criteria for coastal stations used in MLR construction included being close to a
411 coastline, nitracline <40 m depth and chlorophyll maximum larger than 9.5 mg m $^{-3}$. Offshore stations were selected
412 based on furthest distance from a coastline. Not all stations proximal to the coastline were characterized as coastal
413 (see map) nor included in the 'coastal' subset used to train the model (Table S2a, b).

Formatted: No underline, Underline color: Auto

Formatted: No underline, Underline color: Auto

Deleted: 8atm

Deleted: 'coastal'

Deleted: 'offshore'

Deleted: Stations

Deleted: identified

Deleted: 'coastal' or 'offshore',

Deleted: depth

Deleted: 'coastal'

422 ~~Using the same subsets of 'coastal' and 'offshore' stations, a second set of MLR models ('core' models) was built~~
423 using a more limited set of core variables from the PPS data that focused on phytoplankton and nitrifier physiology
424 and metabolism (chlorophyll, nitrate, ammonium, oxygen and percent PAR). These five environmental variables, their
425 quadratic terms and single interaction terms were included for 20 parameters in total. This model experiment was
426 constructed to assess the relative importance of these core variables between 'coastal' and 'offshore' ~~regimes~~
427 therefore, no model size optimization was used to limit variables. Instead, optimized coefficients for all variables were
428 determined, and variables that contributed less than 2% of total R^2 in both regional models were discarded. In two
429 cases, a variable that was discarded from one regional model was added back to keep the variable list identical between
430 both models for ease of comparison. ~~For example, in~~ the coastal 'core' model, the quadratic term for chlorophyll
431 contributed less than 2% to total R^2 but contributed greater than 2% relative importance within the offshore 'core'
432 model, and was therefore retained in both models. In the offshore 'core' model, PAR was initially removed during the
433 optimization processes because it contributed less than 2% to model R^2 , but was ultimately retained because it
434 contributed greater than 2% relative importance within the coastal 'core' model. The relative percent importance of
435 each variable was calculated by iterative random-ordered removal of each variable to estimate percent contribution to
436 total model R^2 using the *relaimpo* package in R (Grömping, 2006).

~~Deleted: A~~

437 3 Results

438 3.1 PNM structure and environmental conditions

439 The typical PNM feature in the ETNP was a unimodal nitrite accumulation situated just below the chlorophyll
440 maximum and at the top of the nitractine (e.g., Fig. 1b, c). The PNM feature can be described using characteristics of
441 the PNM peak (i.e., ~~maximum~~ nitrite ~~concentration~~ (μM) and depth of the nitrite maximum (m)) and an integrated
442 nitrite quantity for the whole PNM feature. Although nitrite can seasonally accumulate all the way to the surface in
443 some regions (Zakem et al., 2018), homogenous surface nitrite concentrations were not observed in this dataset. Across
444 the ETNP study region, stations showed similar relative water column ~~structures~~ in the upper 200 m, although the
445 exact depth and magnitude of features varied. Generally, the depth distribution of features from shallowest to deepest
446 was the top of nitractine, the chlorophyll maximum, the ammonium maximum then the ~~nitrite~~ maximum (Fig. 1b, c).
447 This set of sequential features occurred near the base of the euphotic zone at most stations. Surface irradiance
448 attenuated through the water column and the depth of 0.1-1 % surface PAR ranged between 25 m and 150 m depth,
449 with the deepest light penetration at offshore stations. The chlorophyll maximum was usually found around the 1%
450 surface PAR depth and within the nitractine. However, there was variation in how deep the chlorophyll maximum sat
451 within the nitractine, as reflected in the amount of nitrate measured at the depth of the chlorophyll maximum (Table
452 S2a). The depth of the nitrite maxima tended to occur within the downslope of the chlorophyll maxima. The depth
453 horizon of the PNM was often narrow, with detectable nitrite concentrations spanning only 30 m in some cases.

~~Deleted: .~~

~~Deleted: maximum~~

~~Deleted: structure~~

~~Deleted: Nitrite~~

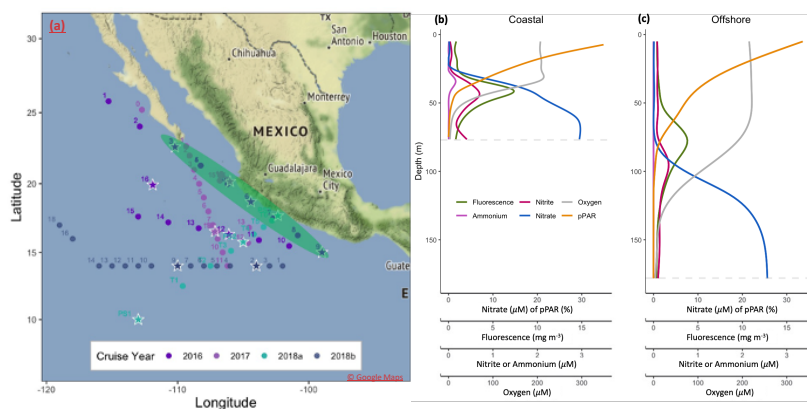
~~Deleted: , while the rest of the water column had very low concentrations of both N species.~~

454 The depth of maximum nitrite in the PNM shoaled from an average depth of 103 m at offshore stations to 21 m near
455 the coast, closely following the shoaling nitractine. In density space, the depth of the nitrite maxima fell within a

~~Formatted: Space After: 11.85 pt~~

465 narrower range, from 22.1 to 26.3 kg m^{-3} , with a mean density across the study region of 24.1 kg m^{-3} . The nitrite
 466 maxima had an average concentration of ~600 nM, but a range spanning 60-1520 nM. Two types of stations ('coastal'
 467 and 'offshore') were identified based on water column features. Coastal stations (e.g., 2016 PPS 6, 7, 8, 9) had higher
 468 concentrations of nitrite at the nitrite maxima, shallower depths of the nitrite maxima, more nitrate and slightly more
 469 chlorophyll and light at the depth of the nitrite maxima (Table. S2a). Coastal stations also had shallower oxyclines,
 470 1% PAR depths, ammonium maxima and chlorophyll maxima compared to offshore stations. Depth-integrated
 471 chlorophyll, nitrate and ammonium in the upper 120 m were higher at coastal stations. Offshore stations (e.g., 2016
 472 PPS 13,14, 15,16) had deeper nitraclines, smaller chlorophyll maxima and less light at the depth of the nitrite maxima.

473 **Figure 1.** Map of the ETNP region showing cruise tracks included in this study from 2016-2018 (a).
 474 Stations where rate measurements were made are marked with white stars. Pump profile data was collected at each station
 475 occupied during the 2016 cruise, and coastal stations are encircled in green. Mean water column profiles from example
 476 'coastal' stations (8 and 9) and example 'offshore' stations (14 and 16) during the 2016 cruise (b, c). Dashed grey line depicts
 477 the depth at which dissolved oxygen concentrations declined below 3 μM .



478 479 3.2 Regressions with the nitrite maxima

480 There were no strong linear correlations between the concentrations of nitrite and other observed environmental
 481 variables in vertical profiles (chlorophyll, depth, density, oxygen, temperature, nitrate, ammonium). This is
 482 unsurprising since the features with unimodal profiles (chlorophyll, ammonium) have concentration maxima that are
 483 offset vertically from the nitrite maxima, and features with other distributions (e.g. exponential) are not expected to
 484 have linear relationships with a unimodal nitrite profile. However, spatial relationships between environmental
 485 gradients are still observed in the quantity regressions; for example, the density regression clearly shows that the peak
 486 of the PNM feature consistently fell near 24 kg m^{-3} isopycnal across the region in 2016.

487 To better match unimodal nitrite profiles with spatially offset and vertically non-unimodal environmental gradients,
 488 station-specific features were identified in the high-resolution 2016 PPS profiles and, where possible, in the CTD
 489 datasets (Table 1; e.g., concentration of the nitrite maxima and depth of nitrite maxima). The strongest correlation (R^2)

Deleted: 313
 Formatted

Deleted: 314

Formatted: Font: Calibri

Deleted: 315 ...% PAR depths, ammonium maxima and chlorophyll maxima compared to offshore stations. Depth-integrated 316 ...chlorophyll, nitrate and ammonium in the upper 120 m were higher at coastal stations. Offshore stations (e.g., 2016 317

Formatted

Deleted: 318 ...igure 1. Map of the ETNP region showing cruise tracks included in this study from 2016-2018 (a). 319 ...ations where rate measurements were made are marked with white stars. Pump profile data was collected at each station 320 occupied during the 2016 cruise....and coastal stations are encircled in green. Mean water column profiles from example 'coastal' stations (8 and 9) and example 321

Formatted: Font: Times New Roman, 9 pt, Bold

Deleted: 322

Deleted:

Deleted: 323 →

Deleted: 325

Formatted: Font: Calibri

Formatted: Indent: Left: 0", First line: 0"

Deleted: 326 ...ariables in vertical profiles (chlorophyll, depth, density, oxygen, temperature, nitrate, ammonium)

Formatted: Font: Calibri

Deleted: 328 ...ffset vertically from the nitrite maxima

Formatted: Font: Times New Roman

Deleted: 330

Formatted: Font: Calibri

Deleted: 331

Deleted: (Fig. S1).

Deleted: 332

Formatted: Font: Calibri

Deleted: 333

Deleted: 333

Formatted: Font: Calibri

Deleted: 334 ...atasets (Table 1,... e.g., concentration of the nitrite maxima and depth of nitrite maxima)

492 = 0.50, p<0.01) appeared between the concentration of the nitrite maxima (nM) and the nitrate concentration at the
493 nitrite maxima (Fig. 2c). The Brunt-Väisälä frequency (BV), related to water column stability, also had a strong
494 positive correlation ($R^2 = 0.40$, p<0.01) with the concentration of the nitrite maxima (Fig. 2l). There were weaker
495 correlations with other parameters such as the concentration of chlorophyll at the depth of the nitrite maxima (mg m⁻³),
496 the concentration of the chlorophyll maxima (mg m⁻³), temperature (°C) at the depth of the nitrite maxima and
497 oxygen concentration (μM) at the depth of the nitrite maxima ($R^2 = 0.20$, 0.23, 0.25, 0.29, respectively, all p<0.05)
498 (Fig. 2a, h, f). Removing the outliers from the two chlorophyll regressions (Fig. 2a, 2b) did not improve the correlations
499 ($R^2 = 0.06$ and 0.09 , respectively). The nitrite maxima were not linearly correlated with percent surface PAR (%) at
500 the depth of the nitrite maxima or the concentration of ammonium (nM) at the depth of the nitrite maxima (Fig. 2g,
501 d). Depth-integrated chlorophyll, nitrate, and nitrite concentrations in the upper 120 m (excluding ODZ waters with
502 $O_2 < 3 \mu M$) were higher when the nitrite maximum was larger (Fig. 2i, j, k). The nitrite maxima did not correlate with
503 depth-integrated ammonium concentrations (not shown, see Table S2c for Pearson correlations and p-values).
504 Inclusion of lower resolution CTD casts from cruises in 2017/2018 decreased the strength of the linear correlations,
505 likely because of larger error in determining the depths of water column features (e.g., depth of the nitrite maxima,
506 top of nitracline) with larger (~10 m) spacing between discrete measurements (Fig. S1a).

507 **Figure 2. Linear regressions of maximum nitrite concentrations against those of other parameters, integrated amounts of**
508 **chlorophyll and DIN, and Brunt-Väisälä frequencies using PPS station data from 2016 (n=16).** Chlorophyll concentration
509 at the depth of the nitrite maxima (a), concentration of the chlorophyll maxima (b), nitrate concentration at the depth of
510 the nitrite maxima (c), ammonium concentration at the depth of the nitrite maxima (d), concentration of the ammonium
511 maxima (e), oxygen concentration at the depth of the nitrite maxima (f), percent surface irradiance at the depth of the nitrite
512 maxima (g), temperature at the depth of the nitrite maxima (h), integrated chlorophyll through the top 120 m (i), integrated
513 nitrate through the top 120 m (j), integrated nitrite through the top 120 m (k), and the Brunt-Väisälä frequency across the
514 density gradient ±8 m around the depth of the nitrite maxima (l).

Deleted: concentrations

Deleted: 337

Deleted: 338

Formatted: Font: Calibri

Deleted: 339

Deleted: 340

Deleted: 1

Deleted: 04

Deleted: 1

Formatted: Superscript

Deleted: 343

Deleted: 344

Deleted: 345

Formatted: Font: Calibri

Deleted:).

Deleted: 346

Formatted: Font: Times New Roman

Deleted: 347

Formatted: Font: Times New Roman

Formatted: Font: Calibri

Deleted: 348

Deleted: S2a

Deleted: 349

Deleted: regression

Deleted: concentration of the

Deleted: maxima against

Deleted: of water column features, 350

Deleted: 351

Formatted: Font: Calibri, 10 pt, Not Bold

Deleted: 352

Formatted: Font: Calibri, 10 pt, Not Bold

Deleted: 353

Deleted: 354

Deleted: 355

Deleted: 120m

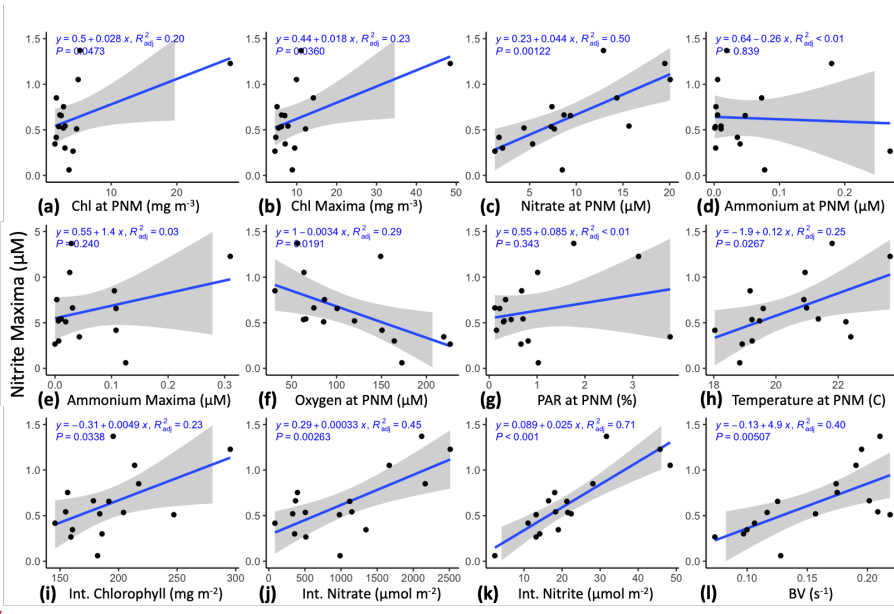
Formatted: Font: Calibri, 10 pt, Not Bold

Deleted: 120m

Deleted: 120m

Deleted: 356

Deleted: 8m



Deleted: 357 →

Deleted: 358 →

Deleted: 359

Deleted: 360

Deleted: 361

Deleted: 362

Deleted: Correlation

Deleted: was

Formatted: Font: Calibri

Deleted: 364

Formatted: Font: Calibri

Deleted: 365

Deleted: depth locations

Deleted: 366

Formatted: Font: Calibri

Deleted: S3

Deleted: 367

Formatted: Font: Times New Roman

Deleted: 368

Deleted: S2b

Deleted: 369

Formatted: Font: Times New Roman

Deleted: 370

Deleted: 371

Formatted: Font: Calibri

Deleted: 372

Deleted: .

Deleted: 373

Deleted: 374

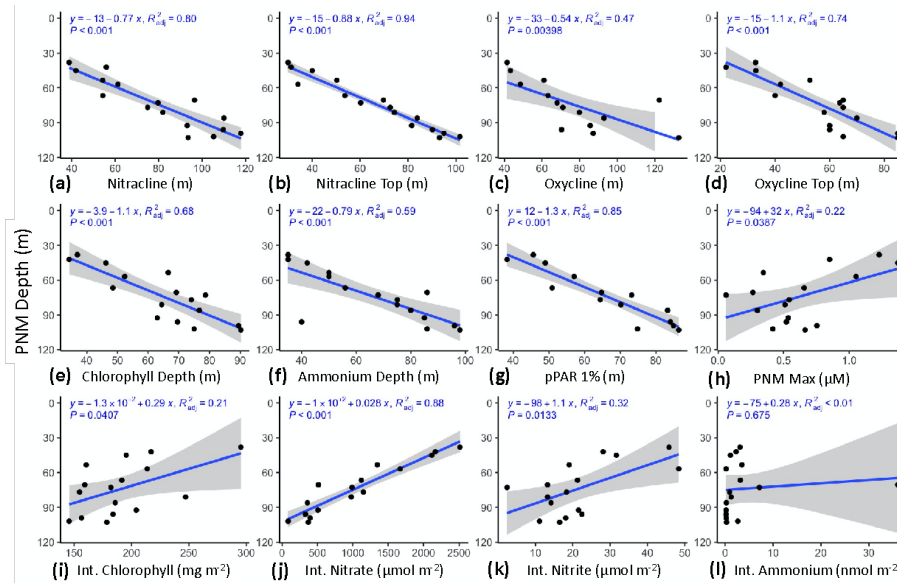
515

3.3 Regressions with depth of the nitrite maxima

The depth of the nitrite maximum at each station was also regressed against the depth of station-specific features (Fig. 3). All water column features showed strong linear correlations with the depth of the nitrite maxima (Fig. 3 a-h). The top of the nitracline and the depth of 1% PAR had the strongest correlations with the depths of the nitrite maxima ($R^2 = 0.94, 0.85$) (Fig. 3b, g). Correlations of depths of the nitrite maxima with midpoint-calculated oxyclines and nitraclines were weaker, possibly because those features are less easily defined, or the steepness of these “clines” were still actively being shaped by the biological responses to changing physical and environmental forcing. The depths of the nitrite maxima tended to be related to the depths of other features and were not as strongly correlated with the magnitudes (concentrations) of any other feature (Fig. S2). However, the depth of the nitrite maxima and the concentration of the nitrite maxima were mildly correlated ($R^2 = 0.22, p = 0.039$), with larger nitrite maxima tending to occur at shallower depths. This correlation became insignificant when the CTD data were included (Fig. S1b). Integrated nitrate had a strong correlation with the depth of the nitrite maxima ($R^2 = 0.88, p < 0.01$), which is reflective of the depth of the nitrite maximum tracking with the top of the nitracline. Depth-integrated chlorophyll and nitrite concentrations had more moderate correlations with the depths of the nitrite maxima ($R^2 = 0.21, p = 0.041$ and $R^2 = 0.32, p = 0.013$, respectively). Depth-integrated ammonium concentrations did not correlate with the depth of the nitrite maxima (see Table S2c for Pearson correlations and p-values).

Figure 3. Linear regression of depths of the nitrite maxima against water column features from data collected during the 2016 cruise using the PPS. Depth of the nitrite maxima was regressed against: a) nitracline depth (m), b) top of the nitracline

534 (m), c) oxycline depth (m), d) top of the oxycline (m), e) depth of the chlorophyll maxima (m), f) depth of the ammonium
 535 maxima, g) depth of 1% surface irradiance, h) concentration of the nitrite maxima (μM), i) integrated chlorophyll through
 536 the top 120 m, j), integrated nitrate through the top 120 m, k), integrated nitrite through the top 120 m and l) integrated
 537 ammonium through the top 120 m. PPS station data from 2016 (n=16).



538

539 3.4 Nitrite Cycling Rates

540 Rates of nitrite cycling determined for the four major nitrite cycling processes near the PNM were within the same
 541 range as previous measurements made in the ETNP region and along the adjacent California coast (Beman et al., 2008;
 542 Santoro et al., 2013, 2010; Ward et al., 1982). Within our dataset, the mean rates of ammonia oxidation and nitrite
 543 oxidation were similar to each other (24.3 ± 3.6 and 19.5 ± 3.4 nM day⁻¹, respectively), although there was a large range
 544 in individual rate measurements across stations and depths, with maximum rates reaching 90.4 and 87.4 nM day⁻¹
 545 respectively. Rates of the two phytoplankton-dominated processes were generally lower and not as similar to each
 546 other, with a mean nitrate reduction rate of 6.1 ± 1.9 nM day⁻¹ and mean nitrite uptake rate of 19.0 ± 5.3 nM day⁻¹.
 547 However, nitrite uptake reached one of the highest rates measured, at 165 nM day⁻¹, and the nitrate reduction rate
 548 reached 53.2 nM day⁻¹ at a coastal station during the 2017 winter cruise. Comparison of mean nitritification rates
 549 between coastal and offshore stations did not show a significant difference (Table S1c). The pooled mean standard
 550 deviation across experimental bottle replicates for ammonia oxidation, nitrite oxidation and nitrate reduction were 3,
 551 4.6 and 1 nM day⁻¹, respectively (Table S1).

Deleted: 375
 Deleted: 376

Formatted: Font: Calibri, 10 pt, Not Bold

Deleted: 377

Deleted: 120m

Deleted: 120m

Deleted: 120m

Deleted: 378

Deleted: 120m

Formatted: Font: 9 pt, Bold

Deleted: 379 → [79]

Deleted: 23

Deleted: 7

Deleted: 5

Deleted: 4

Deleted: 0

Deleted: 85

Deleted: 3

Deleted: 81

Deleted: 0

Deleted: based

Deleted: nitrite uptake rate of 19.0 ± 5.3 nM day⁻¹ and mean

Deleted: .

Deleted: 1

Formatted: Not Highlight

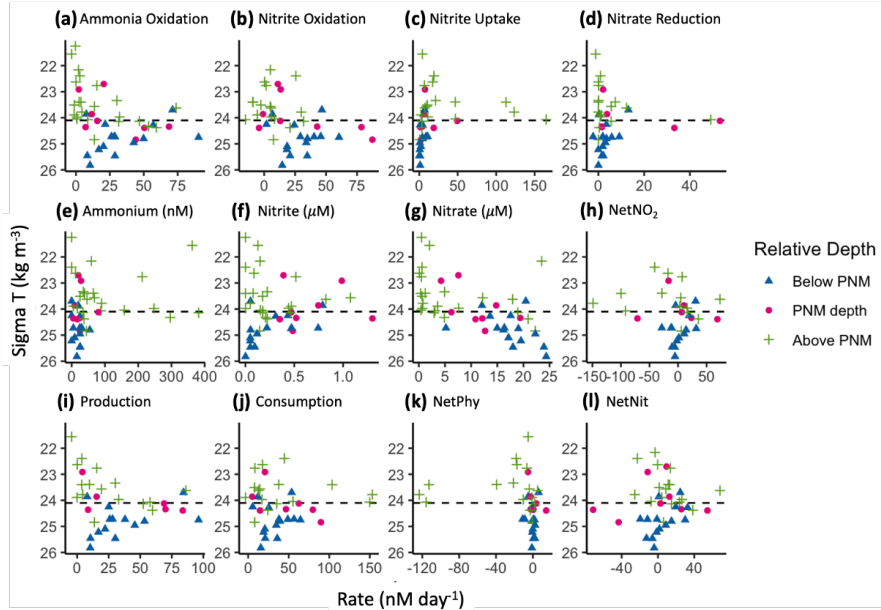
Deleted:

Figure 4. Aggregated rate measurements from 2016-2018 with respect to density (σ T); ammonia oxidation, nitrite oxidation, nitrite uptake and nitrate reduction (panels a-d, respectively) (nM day^{-1}), ammonium (nM), nitrite and nitrate (μM), and net nitrite production (nM day^{-1}) (panels e-h, respectively), and net consumption, net production, net nitrite production from phytoplankton and net nitrite production from nitrification (nM day^{-1}) (panels i-l, respectively). Measurements are colored by relative depth to the station-specific nitrite maximum; above the depth of the nitrite maximum (green crosses), at the nitrite maximum (magenta circles) or below the station-specific depth of the nitrite maximum (blue triangles). The mean ETNP nitrite maxima isopycnal (24.1 kg m^{-3}) is marked as a horizontal dashed line.

Formatted: Left, Indent: Left: -0.01", Hanging: 0.01", Right: 0", Space After: 4.9 pt, Line spacing: Multiple 1.13
li

Deleted: Page Break

Deleted: ¶
maximum (blue triangles). The mean ETNP nitrite maxima isopycnal (24.1 kg m^{-3}) is marked as a horizontal dashed line.



When plotted in density space to aggregate data across years and stations, all processes showed rate **maxima** at a subsurface density layer (Fig. 4). Nitrifier processes (ammonia oxidation (Fig. 4a) and nitrite oxidation (Fig. 4b)), had maximal rates near, or just below, the average density layer for the nitrite maxima across this region (24.1 kg m^{-3}). Nitrite uptake (Fig. 4c) and nitrate reduction (Fig. 4d) rates reached their maxima just above the mean nitrite maxima isopycnal. Nitrification rates were highest in the lower half of the nitractine, while phytoplankton-**dominated** processes (nitrite uptake and nitrate reduction) were highest on the upper slope of the nitractine where **light was available and** nitrite and ammonium concentrations **were higher**. While the highest activities of the two microbial groups were spatially segregated, within-group production and consumption processes had maxima at similar depths. All four rates formed vertically unimodal distributions, but there was still a large range in measured rates near the peaks with many rates close to zero.

585 Net nitrite production from nitrification (NetNit = ammonia oxidation – nitrite oxidation) ranged from -71.5 to 68.4
 586 nM day⁻¹ with a mean of 5.6 ± 3.6 nM day⁻¹ (Fig. 4I). The majority of NetNit values were positive, and maximal rates

Deleted: maximum

Deleted: mediated

Deleted: tended to be

Deleted: and light available

Deleted: alone

Deleted: 49.0

Deleted: 5

Deleted: 1

602 were observed just below the mean nitrite maxima isopycnal. Negative NetNit values were driven by high nitrite
603 oxidation values. Net nitrite production from phytoplankton-dominated processes (NetPhy = nitrate reduction - nitrite
604 uptake) were typically low (mean $-13.3 \pm 4.9 \text{ nM day}^{-1}$), with many negative values resulting from rates of nitrite uptake
605 exceeding those of nitrate reduction (Fig. 4k). The largest negative values occurred above the mean nitrite maxima
606 isopycnal, driven by high nitrite uptake rates where light concentrations were high and nitrate was low in the surface
607 waters. Below the mean nitrite maxima isopycnal, NetPhy remained near zero because both nitrite uptake and nitrate
608 reduction rates were low. The largest positive NetPhy value was at a coastal station (14.4 nM day^{-1}), where nitrate
609 reduction reached 33.4 nM day^{-1} , but NetPhy was typically an order of magnitude smaller than NetNit.

610 The vertical distributions of total nitrite production (production = ammonia oxidation + nitrate reduction, Fig. 4j) and
611 total nitrite consumption (consumption = nitrite oxidation and nitrite uptake, Fig. 4k) showed maximal rates near the
612 mean nitrite maxima isopycnal (24.1 kg m^{-3}). Total nitrite production peaked just below this, with a maximum value
613 of 87 nM day^{-1} . Total nitrite consumption peaked just above it, with a maximum value of 167 nM day^{-1} . The higher
614 consumption rates just above the mean nitrite maxima isopycnal were due to higher nitrite uptake rates, especially at
615 coastal stations (Fig. 4c). There was a large range in rates of nitrite production and consumption processes, but mean
616 values were of similar magnitude (26.4 nM day^{-1} and 39 nM day^{-1} , respectively). Total net nitrite production (NetNO₂,
617 the difference between total production and total consumption) was highest near the PNM. Negative net nitrite
618 production rates could be found both above and below the PNM, reflecting high nitrite uptake above the mean nitrite
619 maxima isopycnal and high nitrite oxidation values below it (Fig. 4h). The mean of positive NetNO₂ values was 16.7
620 nM day^{-1} (rates > -2 only, $n=17$), although mean NetNO₂ was -6.3 nM day^{-1} when all data points were included. The
621 maximum rate of NetNO₂ was slightly higher than NetNit (73.5 vs 68.4 nM day^{-1} , respectively), but the peaks of the
622 vertically unimodal distributions occurred at the same depths.

623 While the aggregated rates of NetNO₂ peaked near the mean nitrite maxima isopycnal for the region, neither NetNO₂
624 (nor any individual rates) were able to predict the observed nitrite concentrations. Simple linear regressions of each
625 rate, or calculated net rates, against the quantity of nitrite did not show significance (Fig. S4). Limiting the regression
626 to a single nitrite maximum and a single highest rate per station also did not show any linear correlation (Fig. S5).
627 However, some qualitative patterns were noticeable, where the highest rates of phytoplankton-dominated processes
628 occurred in samples with lower nitrite concentrations (shallower in the water column). The highest nitrite uptake rates
629 ($>25 \text{ nM day}^{-1}$) appeared to co-occur with maximum nitrite concentrations below 500 nM . Conversely, when high
630 nitrite concentrations were measured ($>600 \text{ nM}$), nitrite uptake rates were low (never higher than 10 nM day^{-1}). Nitrate
631 reduction rates were also higher at lower nitrite concentrations. In addition, the highest ammonia oxidation rates (>40
632 nM day^{-1}) were found where nitrite concentrations were $<500 \text{ nM}$ (Fig. S4). Interestingly, nitrite concentrations were
633 highest ($>600 \text{ nM}$) where ammonia oxidation rates were lower ($<40 \text{ nM day}^{-1}$). The highest nitrite concentrations were
634 associated with waters having lower nitrite oxidation rates ($<20 \text{ nM day}^{-1}$), indicating a low rate of nitrite consumption.
635 Thus, although nitrification was an important contributor to total nitrite production, the balance of processes was more
636 important than the rate of any single process.

Deleted: that were generally higher than

Deleted: 2

Deleted: the mean nitrite maxima isopycnal

Deleted: the mean nitrite maxima isopycnal

Deleted: occurred throughout the whole water column

Deleted: the mean nitrite maxima isopycnal

Deleted: 14.2

Deleted: lower

Deleted: alone

Deleted: 46.9

Deleted: 54.5

Formatted: Subscript

Formatted: Subscript

Deleted: based

Deleted: restrict the

Deleted: quantity

Deleted: ,

Deleted: .

Deleted: The

Deleted: Nitrite

Deleted:

Deleted: although there were more outliers in this regression....

Deleted: instantaneous rates could not be used to predict nitrite concentrations nor could maximum rate at a station predict...

Deleted: nitrite concentration at the nitrite maxima

662 ~~If we assume~~ approximate steady state for PNM nitrite concentrations, rate measurements can be used to calculate a
663 potential residence time for nitrite across the PNM feature. Using total nitrite production and nitrite concentrations,
664 the mean residence time was 30.4 days, ~~while the median residence time was 7.8 days~~. However, there was a wide
665 range in residence times across all samples, particularly those from above the average nitrite maxima isopycnal for
666 the region (Fig. S6a). Using total consumption rates in the calculation gave a slightly lower mean residence time for
667 the region (20.3 days), ~~but again had a large range in residence times above the mean nitrite maximum isopycnal (0.01-103.2 days) (Fig. S6c). Our estimates of average residence time using potential rates may be underestimated~~
668 ~~because of rate enhancement from tracer additions, and we are also likely missing an input/output term from physical~~
669 ~~mixing, which could have a larger influence in dynamic coastal waters compared to offshore. Comparing coastal and~~
670 ~~offshore stations, the estimated residence times are quite different between regimes (mean residence times of 17 and~~
671 ~~53 days, respectively, and median residence times of 5.8 and 18.2 days, respectively) suggesting that coastal nitrite~~
672 ~~accumulations are turning over more quickly even with the limitations and assumptions of these calculations.~~ The
673 discrepancy in residence times calculated using the influx and outflux terms for the nitrite pool suggests that the PNM
674 feature was most likely not in steady state (as also suggested by the high variation in measured rates ~~across~~ the PNM
675 and inability of rates to correlate with observed nitrite accumulation), with differences in the dynamics above and
676 below the nitrite maxima. ~~Additional methods of estimating nitrite age, such as using variation in natural abundance~~
677 ~~nitrite isotopes, may provide more insight (Buchwald and Casciotti, 2013).~~

~~Deleted: Assuming~~

~~Deleted: .~~

~~Deleted: maxima isopycnal (0.01-103.2 days) (Fig. S6c).~~

~~Formatted: Font color: Text 1~~

~~Formatted: Font color: Text 1~~

~~Deleted: at~~

679 3.5 Contribution from Nitrification

680 In considering the metabolisms responsible for accumulation of nitrite at the PNM, it is important to consider the
681 distribution and magnitude of nitrite production processes vertically through the water column as well as their relative
682 contributions to total nitrite production. At our sites in the ETNP, ammonia oxidation contributed over 70% of the
683 total nitrite production through most of the water column (Fig. 5a). The stations where ammonia oxidation contributed
684 less to total nitrite production were typically coastal stations with low ammonia oxidation rates (e.g., <2 nM day $^{-1}$) or
685 with high nitrate reduction rates (>20 nM day $^{-1}$). These results support the idea that both ammonia oxidation and nitrate
686 reduction can contribute to nitrite production, but that the dominant source was from ammonia oxidation at most
687 stations, particularly at the depth of the nitrite ~~maximum~~ and below. For nitrite consumption, nitrite oxidation
688 contributed greater than 70% of total nitrite consumption below the mean density layer of the nitrite maxima. Above
689 ~~this density layer, the contribution to total nitrite consumption from nitrite oxidation became more variable, but with~~
690 most values below 70% due to more nitrite uptake. Particularly low contributions to total nitrite consumption from
691 nitrite oxidation were seen above the depth of the nitrite maxima at coastal stations where nitrite uptake rates were
692 highest. Potential decoupling of ammonia and nitrite oxidation could be seen in the upper water column, with NetNit
693 peaking at the depth of the nitrite maxima (Fig. 4l), which is more difficult to discern in the individual ammonia
694 oxidation and nitrite oxidation rates (Fig. 4a, b).

~~Deleted: maxima~~

~~Deleted: the mean~~

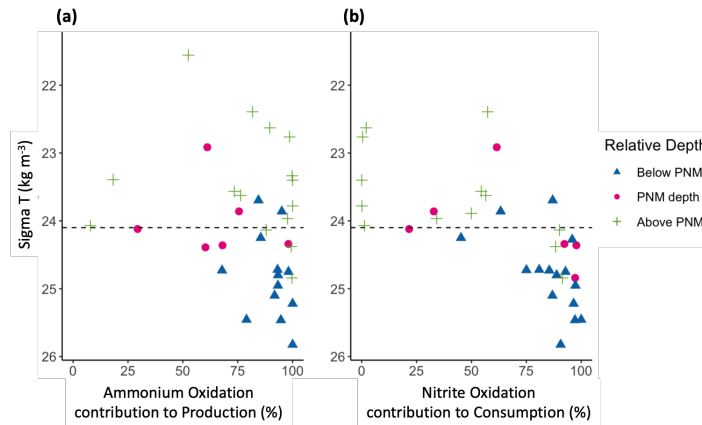
~~Deleted: of the nitrite maxima~~

~~Deleted: Percent contribution~~

~~Deleted: depth~~

695 **Figure 5.** ~~Contributions of nitrification to total nitrite production (a) and total nitrite consumption (b) across density space.~~
696 ~~Measurements are colored by depth relative to the station-specific nitrite maximum; above the depth of the nitrite~~

706 maximum (green crosses), at the nitrite maximum (magenta circles) or below the station-specific depth of the nitrite
707 maximum (blue triangles). The mean ETNP nitrite maxima isopycnal (24.1 kg m⁻³) is marked as a horizontal dashed line



708

709 **3.6 Multiple Linear Regression Analyses**

710 **3.6.1 'Full' model PNM predictions**

711 Multiple linear regression analyses using all available variables (i.e. the "full" model) was able to predict the presence
712 of a primary nitrite maximum at most stations when trained using all stations, the coastal station subset, or the offshore
713 station subset (Fig S3). However, variables selected during optimization and the coefficients determined were not
714 consistent across the three full models, and depth and size accuracy of nitrite predictions was highly variable (Table
715 S3, S4).

716 The all-station 'full' model predicted the depth of the nitrite maxima well (mean depth error = 3.7 m) but
717 underpredicted the maximum nitrite concentration by an average of 230 nM across all stations (after the extreme over-
718 prediction of 15 μ M at Station 8 was omitted) (Fig. S3, Table S4). Retraining the model using a subset of coastal
719 stations improved fit for the training subset of stations (mean depth error 2.9 m), but was no longer applicable across
720 other stations in the region (Fig S3). When applied to non-coastal stations, the coastal 'full' model overpredicted (>2x)
721 the nitrite maxima (except Stations 10,11,12), with an average overprediction for the whole region of ~1.13 μ M (Table
722 S4). Similar results were found when the model retrained using the offshore subset of station. The offshore 'full'
723 model predicted the depth of the nitrite maxima well for offshore stations, with a mean underprediction in depth of
724 only 0.3 m (Fig. S3, Table S4), and underpredicted the maximum nitrite concentration at offshore stations by only 53
725 nM on average. The mean overprediction of nitrite concentration by the offshore 'full' model applied across all
726 stations was 855 μ M, driven by an extreme overprediction at Station 8, which when excluded, makes the mean size
727 error only 1.23 μ M.

Deleted: using all stations

Formatted: Indent: First line: 0"

Deleted: The 'full' model multiple linear regression optimization across all stations resulted in a combination of 10 variables that were able to predict 66% of the total variance in nitrite concentration (Fig S7a). The final optimized model included 3 primary variables (chloro... [80]

Deleted: and

Deleted: maxima

Deleted: when

Deleted: 6

Deleted: The accuracy of

Deleted: all-station

Deleted: varied across station types, with the most ac... [81]

Deleted: , offshore and other (3,4 10,11,13). [82]

Deleted: the coastal model (6, 7, 8, 9) are boxed in [83]

Deleted: of the nitrite maxima well at the coastal stat... [84]

Deleted: (Fig. 6, Table S4). The concentration at the... [85]

Formatted: Font: 10 pt, Not Bold

Formatted: Font: 10 pt, Not Bold

Formatted: Font: 10 pt

Formatted: Font: 10 pt

Formatted: Font: 10 pt

Deleted: The inability of this model to be applied ac... [86]

Formatted: Font: 10 pt

Deleted: 6

Deleted:). The offshore model

Deleted: of the nitrite maxima

Formatted: Font: 10 pt

Formatted: Font: 10 pt

Formatted: Font: 10 pt

Formatted: Font: 10 pt

Deleted: Predicted

Deleted: profiles accurately captured the

Deleted: of the nitrite maxima at offshore stations 13... [87]

Formatted: Font: 10 pt

Formatted: Font: 10 pt

Formatted: Font: 10 pt

Formatted: Font: 10 pt

Deleted: The offshore model predicts a slight double... [88]

Formatted: Font: 10 pt

841 This set of 'full' variable models showed that there is enough information in the environmental data to make
 842 correlative predictions of nitrite profiles, but also showed regional variability precludes a single model for the region.
 843 Additionally, investigating model variables and coefficients to gain insight on environmental controls of the PNM is
 844 difficult when different variables are used in each version of the model.

845 **3.6.2 'Core' model PNM predictions**

846 A subset of 'core' variables was selected and applied in a second set of MLR analyses in order to directly compare the
 847 influence of each variable on nitrite concentration between two regions (coastal vs. offshore) (See Methods). The 'core'
 848 models limited variables to those that had strong single linear regressions with depth and concentration of the nitrite
 849 maxima, and both the coastal and offshore models explained similar amounts of the total variance in nitrite
 850 concentration in their respective regions. Even though both models explained relatively similar amounts of variation
 851 in nitrite concentration and used the same limited suite of variables, different coefficients led to differing predicted
 852 nitrite profiles across stations (Fig. 6, Table 2). In the coastal region, the primary model components included nitrate
 853 and light, two environmental variables that are related to initiation of bloom conditions. The offshore model shifted
 854 importance slightly towards a stronger chlorophyll component and reduced the importance of light. In both regional
 855 models, nitrate was involved in explaining the most variance (40.8% in the coastal model, 38.8% in the offshore
 856 model).

857 Table 2. Coefficients and relative importance from core models; coastal (a) and offshore (b).

(a) Coastal 'Core' MLR Coefficients			(b) Offshore 'Core' MLR Coefficients		
Variable	Coefficient	Percent Importance	Variable	Coefficient	Percent Importance
Oxygen-Nitrate	0.0028	18.9	Chl-Nitrate	0.0752	16.7
Nitrate	-0.4137	12.2	Oxygen-Nitrate	0.0029	11.9
pPAR	-0.0183	12.1	Chlorophyll	0.46	11.1
Chl-Nitrate	0.0538	9.7	Oxygen	-0.0124	11
Chlorophyll	-0.0837	4.6	Nitrate	-0.7093	10.2
Oxygen	-0.0047	4.6	Chlorophyll2	-0.0994	6.8
Chlorophyll2	-0.0014	2.3	pPAR	-0.0012	4.4

858 In general, the coastal 'core' model predicted the depth of the PNM well, but was less accurate in predicting maximum
 859 nitrite concentration, and peak shape (Fig. 6). The coastal 'core' model underpredicted the depth of the nitrite maxima
 860 at coastal stations (-1.7 m), and underpredicted coastal nitrite maxima by an average of 208 nM, with a large range in
 861 error (-830 to +811 nM) (Table S5). Applying the coastal model to the full set of 16 stations showed that the coastal
 862 'core' model could either overpredict or underpredict the nitrite maximum at non-coastal stations, in addition to
 863 predicting a wide PNM shape that extends deeper in the water column than observed (Fig. 6). The predicted depths of
 864 the nitrite maxima from the coastal model fit well with the depths of the observed nitrite maxima, with a mean depth
 865 overprediction of only 2.3 m, a single large outlier at Station 1 was observed, where PNM depth was overpredicted
 866 by 23.4 m (Fig. 6, Table S5).

Deleted: 3.7 Multiple Linear Regression – 'core' model
 PNM

Moved (insertion) [7]

Deleted: MLR analysis in order to directly compare the influence of each variable between two regions (Coastal vs Offshore stations) (See Methods). There were 7 variables included in the final 'core' models, with 4 primary variables, 1 quadratic term and 2 interaction terms (Table 2).

Formatted: Font: Bold

Deleted: (a) (b)
 - Coastal 'Core' MLR Coefficients - Offshore 'Core' MLR Coefficients
 - Variable Coefficient Percent Importance Variable Coefficient Percent Importance
 - Oxygen-Nitrate -0.0028 -18.9 Chl-Nitrate -0.0752 -16.7
 - Nitrate -0.4137 12.2 Oxygen-Nitrate -0.0029 -11.9
 - pPAR -0.0183 12.1 Chlorophyll -0.46 -11.1
 - Chl-Nitrate 0.0538 9.7 Oxygen -0.0124 -11
 - Chlorophyll -0.0837 -4.6 Nitrate -0.7093 10.2
 - Oxygen -0.0047 -4.6 Chlorophyll2 -0.0994 6.8
 - Chlorophyll2 -0.0014 -2.3 pPAR -0.0012 -4.4

3.7.1 Coastal 'core' model

The coastal 'core' model was able to explain 83% of the variance in coastal nitrite concentration. The top 3 variables (oxygen-nitrate, nitrate, and pPAR) explained over half of the total model variance (44.1%). Nitrate was the dominant variable, with the combined contribution of all 3 nitrate variables explaining 41.9% of model variance. The total contribution of the chlorophyll related variables was 17.5%. The slope of the predicted vs observed values was 0.71, less than 1, indicating a tendency to overpredict the size of smaller nitrite maxima (<~350 nM) and underpredict larger sized nitrite maxima (Fig. S8a).

Deleted: for

Deleted: maxima

Deleted: general

Deleted: 7

Deleted: overpredicted and underpredicted

Deleted: maxima

Deleted: as well as

Deleted: 7

Deleted: this

Deleted: depth

Deleted: , with

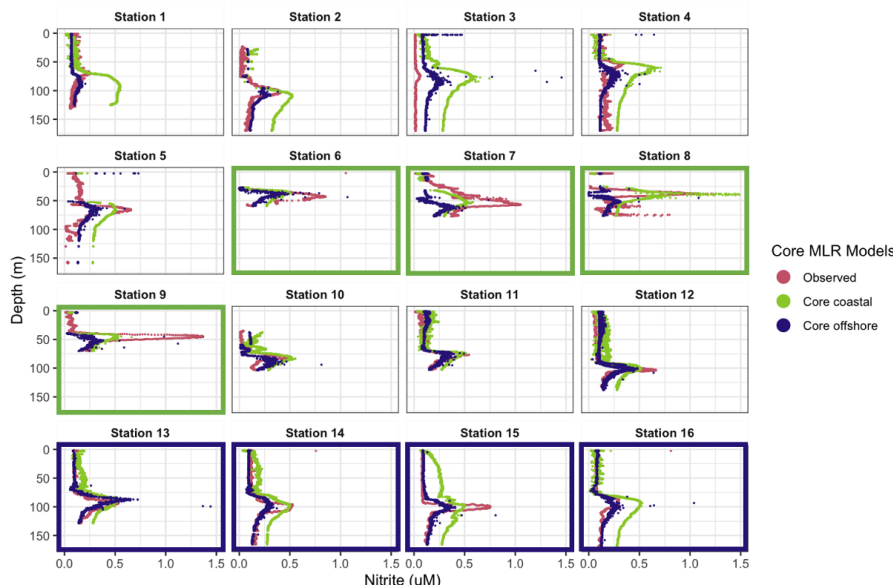
Deleted: 7

Deleted: On average, the coastal model overpredicted the nitrite maxima by just 12 nM across the region. However, there is a wide range in direction of prediction error, with Station 8 being overpredicted by 810 nM and Station 9 underpredicted by 830 nM.

916 The offshore 'core' model also predicted the depth of the nitrite maxima well, but less accurately predicted the
 917 concentration of the nitrite maxima (Fig. 6). The depths of the nitrite maxima at offshore stations were predicted to
 918 within 2.8 m, but the maximum nitrite concentrations were underpredicted by 82 nM at offshore stations. Applying
 919 the offshore core model across all 16 stations showed that worse on average, giving predicted depths of the nitrite
 920 maximum that were on average 5.5 m deeper than the observed depth, with a range in over- and underpredictions
 921 from 18.6 m to 5.5 m respectively. The predicted concentrations of nitrite maxima were lower than observations by
 922 an average of 218 nM across the region (Table. S5).

923 **Figure 6.** Predicted nitrite profiles from 'core' coastal MLR (green) and offshore MLR (blue). Observed nitrite profiles
 924 from PPS 2016 dataset (magenta).

925



927 4 Discussion

928 4.1 Vertical structure of nitrite accumulation

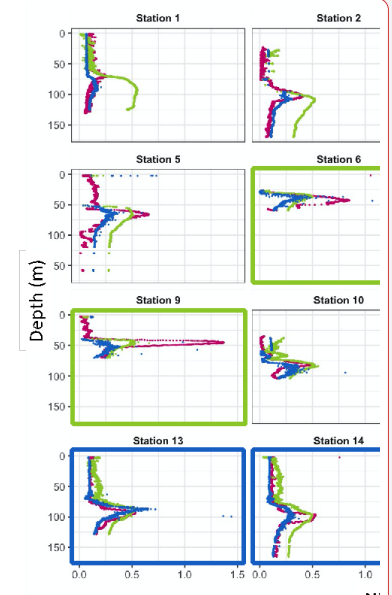
929 The same vertical sequence of water column features was seen at all ETNP stations, with the chlorophyll maximum
 930 lying above the ammonium maximum lying above the depth of the nitrite maximum at the top of the nitractine. These
 931 consistent spatial relationships between water column features suggest that there is a specific set of environmental
 932 conditions and biological agents that lead to the accumulation of nitrite. Linear regressions between depth of the nitrite
 933 maxima and the depth of other key water column features indeed showed strong correlations. Previous work has noted

Deleted: 3.7.2 Offshore 'core' model [\[89\]](#)

Deleted: the offshore core model tended to underpredict the nitrite maxima across the region. The... worse on average, giving predicted depth... depths of the nitrite maxima was an... maximum that were on average of ...5 m deeper than the observed depth of the nitrite maxima... with a range in over- and underpredictions from 18.6 m to 5.5 m respectively. The predicted concentration... concentrations of the ...itrite was...ere lower than observations by an average of 2 ... [\[90\]](#)

Deleted: 4

Deleted: 7.... Predicted nitrite profiles from 'core' coastal MLR (green) and offshore MLR (blue). Observed nitrite profiles from PPS 2016 dataset (deep pink) [\[91\]](#)



Deleted:

Deleted: ...he same vertical sequence of water column features was seen at all ETNP stations, with the chlorophyll maximum lying above the ammonium maximum lying above the depth of the nitrite maxima [\[92\]](#)

997 the connection of the depth of the nitrite maximum with the nitracline (Dore and Karl, 1996; Herland and Voituriez,
998 1979; Lomas and Lipschultz, 2006; Meeder et al., 2012; Shiozaki et al., 2016; Vaccaro and Ryther, 1960) and with
999 the chlorophyll maximum (Collos, 1998; French et al., 1983; Kiefer et al., 1976; Meeder et al., 2012), showing that
1000 these relationships are shared across multiple oceanic regimes. The environmental feature that correlated most strongly
1001 with the depth of the nitrite maximum in our dataset was the top of the nitracline, while the depth of the chlorophyll
1002 maximum, the depth of the ammonium maximum, the depth of 1% PAR and the top of the oxycline also showed
1003 strong correlations, as illustrated by regression analysis (Fig. 3).

1004 The strong covariance between multiple features provides some Insight into the mechanisms that link the depth of the
1005 nitrite maximum to the environment. Nitrite-cycling microbes respond to the differences in environmental conditions
1006 above and below the PNM. In oligotrophic waters, such as those in the offshore ETNP, uptake of nutrients by
1007 phytoplankton maintains low levels of DIN in the upper euphotic zone as physical resupply is low. As light decreases
1008 with depth in the water column, active phytoplankton growth is diminished and ammonium and labile dissolved
1009 organic nitrogen are released due to grazing and decomposition, providing the low-light conditions, ammonium and
1010 reduced organic N substrates suitable for ammonia oxidation. Nitrite oxidizers utilize nitrite produced predominantly
1011 from ammonia oxidation to return nitrate to the system. Above the PNM, where light is available, there is enhanced
1012 potential for nitrite uptake by phytoplankton and nitrite does not accumulate. Below the PNM, there is diminished
1013 supply of ammonium and nitrite oxidizers continue to consume low levels of nitrite produced through ammonia
1014 oxidation. At the depth of the nitrite maximum, production terms outweigh both spatially segregated loss terms
1015 nitrite uptake and nitrite oxidation.

1016 The production of nitrite at the PNM is linked to the vertical structuring of the upper water column qualities and is
1017 both directly and indirectly dependent on phytoplankton activity. It is directly related via the potential for
1018 phytoplankton to release nitrite under varying nitrate supply and light conditions, and indirectly through ammonium
1019 supply provided to the ammonia-oxidizing community. Interestingly, the sequence of events that structures the
1020 nitracline at the base of the euphotic zone (nitrate and light availability \rightarrow uptake of nitrate and phytoplankton growth
1021 \rightarrow formation of the nitracline and oxycline = release of ammonium (and nitrite) \rightarrow oxidation of ammonium by
1022 nitrifiers) is ordered similarly to the strength of the linear relationships with depth of the nitrite maximum (top of
1023 nitracline $>$ %PAR $>$ chlorophyll/ oxycline $>$ ammonium peak depth). The physical processes that change light and
1024 mixing environments initiate the conditions under which phytoplankton and nitrifiers establish their contributions to
1025 the PNM over time. The importance of the time component may help explain why there is variation in the strength of
1026 correlation between instantaneous environmental measurements and a PNM structure that may require weeks to form.
1027 Under more dynamic conditions (e.g., coastal upwelling), our observations are more likely to capture a larger range
1028 in scenarios, from initial upwelling to cessation of upwelling, making correlations between depth of the nitrite
1029 maximum and water column features weaker.

Deleted: maxima

Deleted: with

Deleted: having

Deleted: insight

Deleted: nitrite maximum.

Deleted: conditions

Deleted: -

Deleted: sequential

Deleted: have been forming over

Deleted: ,

1040 **4.2 Concentration of the nitrite maximum**

1041 While the depth of the nitrite maximum is predictable based on features of the water column, the concentration of the
1042 nitrite maximum was more challenging to predict. In regressions of water column features against the concentration
1043 of the nitrite maximum, only the amount of nitrate at the nitrite maximum, the Brunt-Väisälä frequency and the amount
1044 of oxygen at the nitrite maximum had moderate linear relationships ($R^2=0.5$, $p < 0.01$, $R^2 = 0.4$, $p = 0.016$, $R^2 = 0.29$,
1045 $p = 0.019$), while the R^2 values for the other regressions were smaller ($R^2 < 0.25$) (Fig. 2). The connection between the
1046 nitrite maximum and nitrate concentration may reflect the sequence of events that structures the water column and
1047 forms the nitracline (described above). The presence of increased amounts of nitrate at the depth of larger nitrite
1048 maxima suggests that the phytoplankton have yet to deplete nitrate completely, and a large nitrite maximum is
1049 developing during active nitrate uptake at early bloom formation (Collos, 1982; Meeder et al., 2012). At stations with
1050 a large nitrite maximum, there are also higher concentrations of nitrate at the chlorophyll maximum, although the
1051 chlorophyll maximum may still be small (i.e., early bloom). During this time, ammonium production from degrading
1052 and grazed phytoplankton as well as ammonia oxidation to nitrite may co-occur. Under these early bloom conditions
1053 there is potential to accumulate more nitrite due to increased rates of phytoplankton nitrate reduction, high rates of
1054 ammonia oxidation, and/or decrease in loss terms. Controls on the nitrate reduction rate, and the potential for
1055 ammonium competition interactions between phytoplankton and ammonia oxidizers at nitrate replete depths will be
1056 discussed in relation to nitrite cycling rates.

Deleted: phytoplankton

Deleted: a station

Deleted: ie.

1057 The linear correlation between the larger nitrite maxima and stronger density gradients (higher Brunt-Väisälä values)
1058 suggests that decreased loss of nitrite via mixing could contribute to larger accumulation of nitrite at the maximum.
1059 However, degradation of the nitrite maximum by mixing would only move existing nitrite away from the peak depth,
1060 not remove it entirely from the water column.

1061 We took two further approaches to understand the correlative disconnect between environmental conditions and nitrite
1062 maxima, 1) polynomial multiple regression analyses which allow multiple variables to co-explain the depth and
1063 concentration of the nitrite maxima, and 2) making direct measurements of the microbial processes that
1064 mechanistically link environmental conditions to the nitrogen transformation rates leading to nitrite accumulation.

1065 **4.3 Predicting nitrite profiles from environmental dataset**

1066 The lack of strong linear correlations between maximum nitrite concentrations and any single feature may indicate
1067 that multiple conditions need to be met to produce large accumulations of nitrite. For example, earlier work has shown
1068 the largest seasonal nitrite maxima occur at the onset of the deep chlorophyll maximum, where multiple conditions
1069 are met – light is available and nitrate concentrations are still high (Mackey et al., 2011; Meeder et al., 2012).

Deleted: correlation

Deleted: maxima

Deleted: other

Deleted: -

1070 Allowing for multiple environmental conditions to contribute, the ‘full’ multilinear regression models are qualitatively
1071 able to capture the peak shape of the PNM feature using the variables provided, yet are unable to fully explain nitrite
1072 concentration (Fig. S3). For example, the all-station ‘full’ model explained 66% of the overall variance in nitrite
1073 concentration, but the mean error in nitrite maximum predictions was 740 nM with a large range in errors across

Deleted: 6

Deleted: and

Deleted: maxima

1084 stations (-0.84 to 15.28 μM) (Table S4). This large uncertainty is not surprising, since environmental conditions vary
1085 across the ETNP, especially between coastal and offshore stations. The coastal and offshore nitrite maxima were
1086 typically found at similar densities ($\sim 24.1 \text{ kg m}^{-3}$ coastal, $\sim 24.3 \text{ kg m}^{-3}$ offshore), but at coastal stations the average
1087 depth of the nitrite maxima was 43 m shallower, the average nitrate concentration was 3x higher, the average
1088 chlorophyll concentration was 3x higher, average light was 3x higher, oxygen was 25% higher and ammonium
1089 concentrations were also higher (Table S2). This suggests that the nitrite maxima at coastal and offshore type stations
1090 may be innately different, and possibly controlled by different mechanisms. The two 'full' models built using coastal
1091 and offshore subsets were able to explain more of the total variance at those stations ($R^2 = 0.77$ and 0.79, respectively).

1092 The 'core' models, where the variables included in the models were consistent between the coastal and offshore
1093 regimes, were also able to explain a significant portion of the variability in nitrite (R^2 was 0.83 and 0.98, respectively).
1094 Nitrate was a key parameter in both models (Table 2). The smaller chlorophyll coefficients used to model nitrite
1095 maxima at coastal stations make the model less sensitive to large changes in chlorophyll, while the larger offshore
1096 coefficient suggests that small changes in chlorophyll offshore have more influence over the resulting nitrite
1097 predictions. While there was still significant error in the predicted depth and concentration of the nitrite maxima, the
1098 'core' model coefficients show patterns suggesting that nitrite accumulation occurs at depths where chlorophyll, nitrate
1099 and oxygen co-exist, corroborating the findings from that linear regression analyses, that the depth of the chlorophyll
1100 maxima, nitracline top and oxycline top are individually important in determining the depth of the nitrite maximum,
1101 (see Supplement for further comparison of coefficients).

1102 Overall, while the nitrite accumulation in the PNM was predicted moderately well using the environmental conditions,
1103 especially when differentiating between coastal and offshore regimes, the environmental parameters alone were not
1104 able to fully predict nitrite concentrations. Variable physiological responses of the microbial populations involved
1105 with nitrite production and consumption provide a mechanism that integrates multiple environmental parameters into
1106 an observable nitrite accumulation.

1107 4.4 Rates of Nitrite Cycling

1108 Strong single variable correlations with depth of the nitrite maxima and mild correlations with concentration of nitrite
1109 at the nitrite maxima (with supportive findings from the MLR analyses), suggest that while the PNM feature is
1110 consistently linked to specific depths, the maximum concentration of nitrite in a given PNM may be modulated by
1111 more nuanced environmental timings and microbial physiologies. The two main biological mechanistic explanations
1112 for nitrite production at the PNM involve the microbial physiology of phytoplankton and nitrifying bacteria and
1113 archaea. The overlapping habitats and competition for DIN resources requires that we consider both microbial groups
1114 in our understanding of PNM formation (Lomas and Lipschultz, 2006; Mackey et al., 2011; Smith et al., 2014; Wan
1115 et al., 2021, 2018; Zakem et al., 2018). This dataset provides insights into the relative roles of these processes via
1116 direct rate measurements of the four major nitrite cycling processes from the same source water. This allows both
1117 comparison of relative rates of each process within a community and the calculation of net rates of nitrite production
1118 around the PNM feature. Our expectation at the beginning of this study was that higher rates of nitrite production, or

Deleted: Taking subsets of station data to make separate coastal and offshore 'full' models allowed for better explanatory power compared to grouping all of the stations together in a single MLR model (Fig. S7). Model optimization selected different sets of variables to explain the nitrite concentrations in each model, but nitrate was critical across all three models, aligning with results from the simple linear regression analyses, where nitrate is important for explaining both depth of the nitrite maximum and the concentration of the nitrite maximum. While the maximum nitrite concentration was not predicted well by these models, the mean error for the depth of the Nitrite maximum was less than 4 m for all three 'full' models. However, the predicted depth of the Nitrite maximum at individual stations could be more significantly erroneous (Table S4)

Formatted: Font: Not Bold, Not Italic

Moved (insertion) [8]

Moved up [7]: The 'core' models limited variables to those that had strong single linear regressions with depth and concentration of the nitrite maxima, and both the coastal and offshore models explained similar amounts of the total variance in nitrite concentration in their respective regions. Even though both models explained relatively similar amounts of variation in nitrite concentration and used the same limited suite of variables, different coefficients led to differing predicted nitrite profiles across stations (Fig.

Deleted: 7, Table 2). In the coastal region, the primary model components included nitrate and light, two environmental conditions that are related to physical initiation of bloom conditions. The offshore model shifts importance slightly towards a stronger chlorophyll component and reduces the importance of light. The nitrate variables were involved in explaining similar amounts of the nitrite variance in both models (coastal ... [93])

Deleted:

Deleted: The chlorophyll variables are the only coefficients that differ in sign between the two models, with the c ... [94]

Formatted: Indent: Left: 0", First line: 0"

Moved up [8]: The smaller chlorophyll coefficients used to model nitrite maxima at coastal stations make the model less

Deleted: limited

Deleted: the

Deleted: maxima

Formatted: No underline, Underline color: Auto

Formatted: No underline, Underline color: Auto

Formatted: No underline, Underline color: Auto

Deleted: /

Deleted: is particularly unique because we have directly measured...

Deleted: rates

Deleted: , allowing

Deleted: enabling

1219 net nitrite production, would correspond to larger ~~accumulations~~ of nitrite. Our findings, however, revealed a more
1220 complex pattern where the instantaneous rates of gross or net nitrite production did not reflect the amount of
1221 ~~accumulated nitrite. In other words, the imbalance in nitrite production and consumption can indicate whether nitrite~~
1222 ~~concentrations are currently increasing or decreasing, but it provides less predictive power for the instantaneous~~
1223 ~~concentration of accumulated nitrite.~~

~~Deleted: accumulation~~

~~Deleted: observed accumulated nitrite.~~

1224 The spatial distribution of measured rates through the water column showed peaks in each process near the PNM, but
1225 with slight variation in where the rate maxima fell relative to the nitrite maxima. The highest phytoplankton activity
1226 was located just above the PNM peak, while nitrification rates were highest near the PNM peak, a distribution seen in
1227 other nearby systems (Beman et al., 2012; Santoro et al., 2013). Although the aggregated data from the region showed
1228 these spatial segregations by microbial group, this was not always observed at an individual station. The highest rates
1229 of nitrification ~~appear to~~ be slightly skewed towards the lower slope of the PNM, but the depth of the nitrite maximum
1230 at many stations was determined from discrete measurements taken at ~10 m resolution, so it is possible that the real
1231 maxima occurred between sampled depths. The PPS data allowed much more precise determination of the depth and
1232 peak size, although rate measurements were still limited to lower resolution sampling.

~~Deleted:~~

~~Deleted: and distributed in a peak shape~~

~~Deleted: may~~

~~Deleted:~~

1233 The vertical distribution of nitrification has been theorized to be controlled by light inhibition, restricting nitrification
1234 to depths at the base of the euphotic zone (Olson, 1981). However, active nitrification has been observed in the sunlit
1235 surface ocean (Shiozaki et al., 2016; Ward, 2005; Ward et al., 1989), leading to new theories suggesting that ammonia
1236 oxidation is ~~controlled by~~ ammonium or nitrate availability, ~~shifting~~ the competitive balance for ammonium acquisition
1237 away from phytoplankton and towards ammonia oxidizers (Smith et al., 2014; Wan et al., 2018; Xu et al., 2019). In
1238 this dataset, we did measure nitrification rates $>2 \text{ nM day}^{-1}$ at light levels of 25–30% surface PAR at coastal stations,
1239 although there was a clear enhancement of nitrification rates at light levels below 5% surface PAR. Although linear
1240 regressions of ammonia oxidation rate didn't show a strong correlation with the nitrite ~~maximum~~ or depth of the nitrite
1241 ~~maximum~~, there was a relationship between ammonia oxidation and both nitrate and light (Fig. 7). Similar to the data
1242 compiled in Wan et al. (2018), the highest ammonia oxidation rates were restricted to depths with higher nitrate
1243 concentrations and lower light levels. However, even when constraining the ammonia oxidation rate data to where
1244 there is both low light and higher nitrate concentrations, measurements spanned the entire range of rates from 0–85
1245 nM day^{-1} , indicating that the conditions controlling the depth of the rate maxima do not guarantee high rates, but
1246 simply facilitate the possibility of high rates. ~~It should be noted that some of the highest rates were measured in source~~
1247 ~~water with low ambient DIN concentrations, and it is possible that tracer addition relieved DIN-limitation in some of~~
1248 ~~these samples and enhanced the measured rates (Fig S7). However, as these are bulk rates (per volume), we cannot~~
1249 ~~differentiate between potential enhancement of rates due to our tracer addition versus differential microbial~~
1250 ~~abundances.~~

~~Deleted: restricted to near the PNM not only because of inhibition at high light levels, but because~~

~~Deleted: shifts~~

~~Deleted: maxima~~

~~Deleted: maxima~~

~~Deleted: 8~~

~~Deleted:Section Break (Next Page).....~~

~~Deleted: 8.~~

~~Formatted: Font: Calibri, 10 pt. Not Bold~~

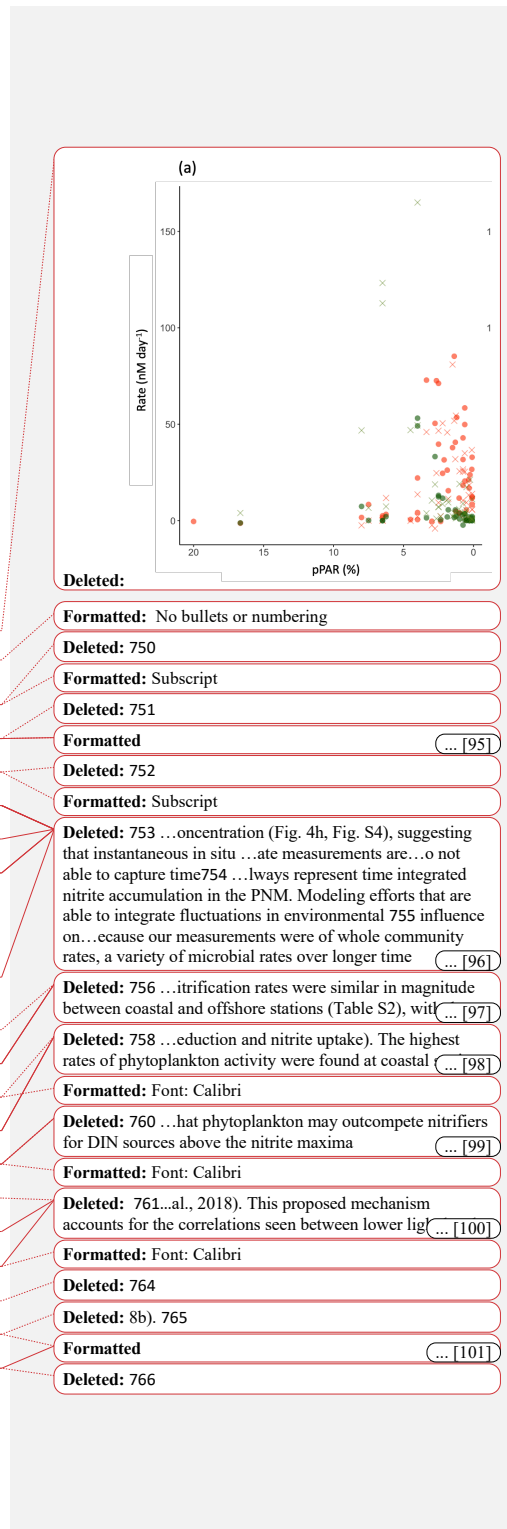
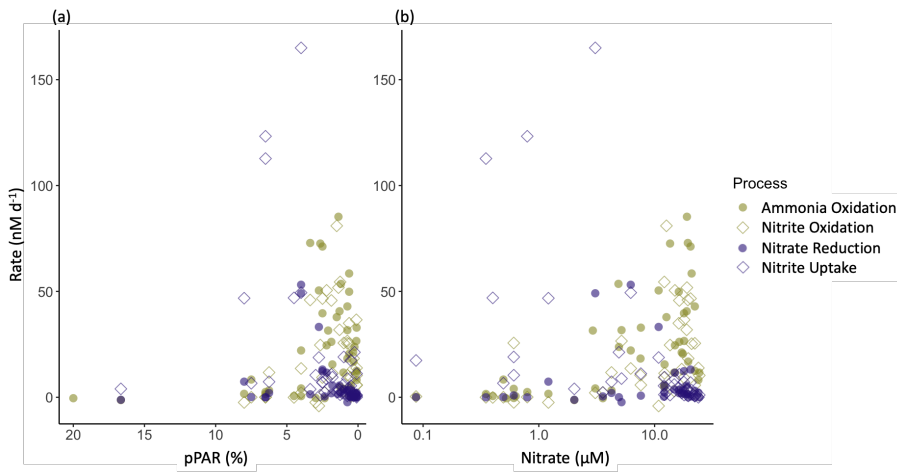
~~Deleted: 746 →~~

~~Deleted: green~~

~~Deleted: orange~~

~~Deleted: consumption processes are x shapes 747 → and~~

1251
1252 **Figure 7** Relationship between nitrite cycling rates and percent surface PAR (a) and nitrate concentration (b).
1253 Phytoplankton-dominated processes are ~~shown in blue~~ and nitrifier processes are ~~shown in green~~. Nitrite production
1254 processes are ~~shown as filled circles and consumption processes are open diamonds.~~



1273

1274 The individual rate measurements were not correlated with the amount of nitrite accumulated in the water column at
 1275 a given depth (Fig. S4). Neither were the net rates (NetNit, NetPhy, NetNO₂) able to explain observed nitrite
 1276 concentrations. Although the vertical pattern in net nitrite production rates (NetNO₂) showed a peak shape that was
 1277 qualitatively similar to nitrite concentration, there was no linear relationship between NetNO₂ and nitrite
 1278 concentration (Fig. 4h, Fig. S4), suggesting that instantaneous rate measurements ~~do not always represent time~~
 1279 integrated nitrite accumulation in the PNM. ~~Because our measurements were of whole community rates, a variety of~~
 1280 ~~microbial processes may have remained active in the incubations alongside the process intended to be traced with~~
 1281 ¹⁵N. For example, the ¹⁵N-NO₂⁺ produced via nitrate reduction is potentially acted upon by nitrite uptake and nitrite
 1282 oxidation. This has the potential of leading to underestimation of nitrate reduction rates, especially where nitrite
 1283 concentrations ~~are low, and nitrite uptake and nitrite oxidation rates are large.~~

1284 Nitrification rates were similar in magnitude between coastal and offshore stations (Table S2), with the major
 1285 differences in ~~rate~~ measurements between coastal and offshore stations found in the phytoplankton-dominated
 1286 processes (nitrate reduction and nitrite uptake). The highest rates of phytoplankton activity were ~~found~~ at coastal
 1287 stations and occurred primarily above the depth of the PNM. The distribution of measured activity lends support to
 1288 the hypothesis that phytoplankton may outcompete nitrifiers for DIN sources above the nitrite ~~maximum~~ (Wan et al.,
 1289 2018; Zakem et al., 2018). This proposed mechanism accounts for the correlations seen between lower lig... [100]

1290 higher ammonia ~~oxidation~~ because the top of the nitracline itself is a physical demarcation of the depth where
 1291 phytoplankton ~~co-~~requirements for light and nitrate are met. Previous work has also shown that the presence of nitrate
 1292 can inhibit nitrite uptake by phytoplankton through competitive interactions (Eppley and Coatsworth, 1968; Raimbault,
 1293 1986) (Fig. 7b). This mechanism may provide a way to connect the presence of nitrate with a larger PNM that relies
 1294 on prevention of nitrite loss, rather than an increase in nitrite production.

1370 An additional loss term that could influence the size of the observed nitrite peak is diffusion, moving nitrite away from
1371 the depth of maximal net nitrite production. In addition to having shallow nitraclines and shallow chlorophyll
1372 maximum depths, as well as larger chlorophyll maxima and nitrite maxima, coastal stations also had the steepest
1373 density gradients near the observed larger PNM, making Brunt-Väisälä (BV) frequency correlate with the nitrite
1374 maxima in this dataset ($p=0.005$) (Fig S9, Fig. 2l). The strong density gradients at the coastal stations (stations 6, 7, 8,
1375 9) would inhibit mixing, potentially allowing for larger concentrations of nitrite to accumulate for a given rate of net
1376 nitrite production. This lack of diffusive loss at coastal stations could partially explain why ammonia oxidation rates
1377 can remain similar between coastal and offshore stations (25.8 ± 3.6 vs. $21.3 \pm 3.3 \text{ nM day}^{-1}$), yet result in higher
1378 accumulated nitrite at a coastal PNM. Modeling efforts that are able to integrate both physical diffusion of nitrite and
1379 mixing around the PNM, as well as the influence of environmental fluctuations on microbial rates over longer time
1380 scales may be more able to explain observed nitrite concentrations. Additional data from time-integrated approaches
1381 such as natural abundance nitrite isotopes would also contribute to estimating nitrite age in the PNM.

1382 4.5 Different time scales inherent to observational patterns

1383 Environmental features may not accurately predict the concentration of the nitrite maximum because of a time lag
1384 between environmental conditions measured at a station, the response of the microbial community, and the length of
1385 time needed to produce a PNM. Previous work has shown that a seasonal PNM can develop over 6 days in the Gulf
1386 of Aqaba (Mackey et al., 2011). In our study, a large range in net production rates was observed ($\sim 0.86.9 \text{ nM day}^{-1}$),
1387 leading to the potential for a PNM to develop in less than a day at some locations, or as long as months at other stations.
1388 The four southern coastal stations (used to inform the coastal MLR) had the largest nitrite maxima measured in this
1389 study (with nitrite concentrations reaching 800-1400 nM). However, it is reasonable to expect that in dynamic coastal
1390 waters, upwelling and offshore transport of water would lead to shorter water residence times and less time for nitrite
1391 to accumulate in the PNM. Indeed, local surface current data from early April 2016 show the fastest currents occurring
1392 along the southern coastline (Fig S8). However, even given these current velocities, nitrite accumulation over the span
1393 of days to weeks seems possible. Thus, our nitrite residence time calculations, on the order of days to months, are
1394 consistent with the residence time of water in the coastal environment, and other estimates of PNM residence times
1395 (Fig. S6). For example, ammonia oxidation measurements from the California Current System suggested an 18-470
1396 day residence time for offshore stations, and 40 day residence time for a coastal station (see full table in Santoro et al.
1397 2013).

1398 4.6 Spatiotemporal controls on the nitrite maximum

1399 Previous work investigating the onset of the PNM has shown that nitrite concentrations are highest at the beginning
1400 of seasonal stratification when phytoplankton begin to bloom, suggesting that phytoplankton help provide the
1401 necessary conditions for nitrite accumulation (Al-Qutob et al., 2002; Mackey et al., 2011; Meeder et al., 2012; Vaccaro
1402 and Ryther, 1960). In Mackey et al. (2011), the onset of stratification initiates a phytoplankton bloom that begins to
1403 deplete surface nitrate and releases ammonia via phytoplankton degradation and zooplankton grazing. An
1404 accumulation of ammonium forms just below the chlorophyll maximum, which is subsequently followed by an

Deleted: may be

Deleted: (both up and down)

Formatted: Indent: Left: 0", Space After: 5.1 pt, Line spacing: 1.5 lines

Deleted: The coastal stations were grouped based on the presence of

Deleted: maxima

Deleted: . In addition to these commonalities, the

Deleted: where gradients are steepest

Deleted: an

Deleted: explain

Deleted: maxima

Deleted: and

Deleted: was observed

Moved (insertion) [9]

Deleted: and months at other stations. However, an imbalance in nitrite production and consumption merely tells you whether nitrite is currently increasing or decreasing, not whether the instantaneously observed nitrite concentration should be high or low. Calculations from rate estimates and isotope data suggest 20-50 day residence times for nitrite in the Arabian Sea PNM (Buchwald and Casciotti, 2013). Ammonia

Moved up [9]: S6.

Deleted: 2013). Our residence time calculations, on the order of days to months, are consistent with these estimates of PNM residence times (Fig.

Deleted: The high variability in accumulation times across sample locations makes it less likely that snapshots of rates and environmental conditions would be representative of conditions for a PNM developing over longer timescales.

Deleted: classic

1435 accumulation of nitrite just below the ammonium peak. This continued stratification pattern supports the persistence
1436 of the emergent PNM feature, though the size of the nitrite maximum declines over the duration of the stratification
1437 period. The correlation between coastal upwelling and higher nitrite accumulation in the ETNP PNM may be
1438 controlled by similar mechanisms as the high nitrite accumulation at the onset of seasonal stratification in other regions.
1439 Instead of a strongly seasonal onset of stratification, the ETNP stratification persists year-round but is modulated by
1440 upwelling along the coast.

1441 At coastal stations in 2016, we saw ~~high~~ average concentrations of nitrate (16 μ M) at the depth of the PNM due to
1442 upwelling conditions, while average nitrate concentrations at offshore PNM were lower (5.9 μ M). The positive
1443 correlation of nitrate concentration at the PNM peak with the concentration of the nitrite maximum ($R^2=0.5$, $p=0.01$)
1444 suggests that upwelling nitrate is critical for larger nitrite maxima. The correlation found in the MLR analysis between
1445 the chlorophyll-nitrate interaction term and the nitrite maxima supports the idea that higher nitrite accumulation
1446 requires the presence of higher levels of nitrate within the chlorophyll bloom. High variation in the correlation of
1447 nitrite maxima with chlorophyll, ammonium and nitrate may be due to how recently the chlorophyll bloom was
1448 initiated, and whether it has had time to draw down available nitrate. However, these patterns do not identify whether
1449 the presence of nitrate drives nitrite production from phytoplankton directly, or indirectly, by stimulating ammonia
1450 oxidation.

1451 Sequential decomposition of particulate organic nitrogen (PON) produces ammonium, then nitrite, and nitrate over
1452 time, and matches the spatial ordering of these species with depth in the water column (Meeder et al. 2012). In a
1453 stratified water column, the vertical transport of material may be slow enough to allow for a similar temporal
1454 degradation pattern to emerge across the pycnocline. The sequence is initiated by the blooming of phytoplankton,
1455 which is restricted to surface depths with adequate light and nitrate. In a coastal upwelling regime, the stratified water
1456 column is pushed up towards the surface, and this degradation sequence is modified by enhanced source PON from
1457 larger chlorophyll blooms. Larger pools of chlorophyll lead to larger ~~accumulations of~~ ammonium and nitrite. Based
1458 on the ~~magnitude of net nitrite production~~, nitrifiers appear to have a larger potential for net nitrite production at ETNP
1459 PNM. The association of nitrification rates with increasing nitrate concentration, which is not a required substrate for
1460 nitrification, indicates an indirect connection with phytoplankton activity which is typically dependent on nitrate
1461 availability. We suggest that changes in light and nitrate availability initiate a cascade of microbial processes that ~~lead~~
1462 ~~from production to degradation of~~ phytoplankton-based PON, providing a substrate for ammonia oxidation. Enhanced
1463 phytoplankton productivity in this scenario should lead to higher rates of nitrite production via ammonia oxidation.

1464 Figure 8. Schematic of nitrite cycling processes and relative DIN pools near the PNM. Panel (a) depicts the
1465 offshore conditions and panel (b) depicts early upwelling conditions that lead to bloom initiation.

Deleted:Section Break (Next Page).....
804 ...t coastal stations in 2016, we saw higher...igh average concentrations of nitrate (16 μ M...6 μ M) at the depth of the nitrite maxima 805
... [102]

Formatted: Font: Times New Roman

Deleted: nitrite maxima

Deleted: 806

Formatted: Font: Times New Roman

Deleted: 807

Formatted: Font: Times New Roman

Deleted: 808

Formatted: Font: Times New Roman

Deleted: 809 ...cumulation requires the presence of higher levels of nitrate within the chlorophyll bloom. High variation in the 810
... [103]

Formatted: Font: Times New Roman

Deleted: 811 ...loom was initiated (... and whether it has the bloom ...ad time to draw down available nitrate?...).
However, these patterns do not identify 812
... [104]

Formatted: Font: Times New Roman

Deleted: 813 ...mmonia oxidation, or is a proxy for a more stratified water column
... [105]

Deleted: 814 ...sequential decomposition of particulate organic nitrogen (PON) produces ammonium, then nitrite, and nitrate over 815
... [106]

Deleted: 816

Formatted: Font: Times New Roman

Deleted: 817 ...degradation pattern to emerge across the pycnocline. The sequence is initiated by the blooming of phytoplankton, 818
... [107]

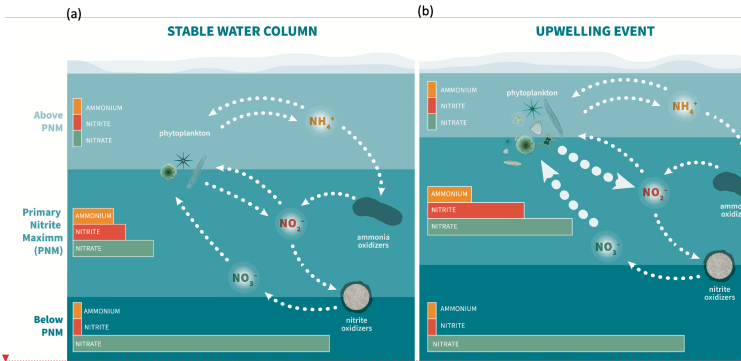
Formatted: Font: Calibri

Deleted: 819 ...olumn is pushed up towards the surface, and this degradation sequence is modified by enhanced source PON from 820 ...arger chlorophyll blooms. Larger pools of chlorophyll lead to larger accumulations of ammonium and nitrite accumulation... Based on 821 ...he magnitude of net nitrite production attributed to phytoplankton vs. nitrifiers... nitrifiers appear to have a larger 822...potential for net nitrite production at ETNP PNM. The association of nitrification rates with increasing nitrate 823 ...oncentration, which is not a required substrate for nitrification, indicates an indirect connection with phytoplankton 824 ...ctivity which is typically dependent on nitrate availability. We suggest that changes in light and nitrate availability 825 ...nitrate a cascade of microbial processes that degrade...lead fr... [108]

Deleted: 827 ->

Deleted: 9.... Schematic of nitrite cycling processes and relative DIN pools near the PNM feature... Panel
... [109]

Formatted: Indent: Left: -0.01", First line: 0"



Deleted: 829 →

Formatted: Justified, Indent: Left: -0.01", Hanging: 0.01", Right: 0.18", Space After: 10.7 pt, Line spacing: Multiple 1.05 li, Tab stops: Not at 3.23"

Deleted:Section Break (Next Page).....

Deleted: 9

Deleted: a

Deleted: 9a

Deleted: 9b

Deleted: 9a

Deleted: coming

Deleted: 9b

1572

1573

1574 Figure 8 places the findings in the current study in the context of the sequential physical and biological processes
 1575 controlling the PNM feature in the ETNP. The schematic depicts a typical offshore PNM from our study region
 1576 observed during stratified, stable water column conditions (Fig. 8a), in contrast to that observed during the onset of
 1577 upwelling (Fig. 8b). In each case, the surface ocean is split into 3 layers: above, within, and below the PNM, with the
 1578 PNM sitting near the top of the nitracline. Phytoplankton control the availability and supply of DIN above the PNM,
 1579 where high light allows for complete drawdown of DIN. In the stable water column (Fig. 8a), phytoplankton are
 1580 present in a chlorophyll maximum that is small and stable just above the nitracline consisting of smaller eukaryotes
 1581 and cyanobacteria (Legembre-Fixx, 2017). The chlorophyll maximum is small because there is no active upwelling,
 1582 and the ambient nitrate at the chlorophyll maximum has been depleted to low concentrations. Phytoplankton fail to
 1583 access deeper nitrogen supplies because light levels become inadequate at depth, so the chlorophyll maximum is
 1584 balanced at the intersection of the dual requirements for light and upwardly diffused nitrate. A small ammonium peak
 1585 develops just below the chlorophyll maximum, and just above the nitrite maximum, deriving from phytoplankton
 1586 decomposition processes including grazer activity. The supply of ammonium is adequate to fuel an active nitrifier
 1587 community in the PNM layer and below, with average rates of ammonia oxidation and nitrite oxidation near 20 nM
 1588 day⁻¹. The net imbalance in the two steps of nitrification is small (few nM day⁻¹), contributing to the small yet stable
 1589 accumulation of nitrite at the PNM. Contributions of nitrite from phytoplankton are minimal because they have drawn
 1590 down surface nitrate and are subsisting at the edge of a well-established deep nitracline. Although the water column
 1591 is stably stratified, the Brunt-Väisälä values are moderate.

1592 During an upwelling event (Fig. 8b), an influx of nitrate-rich water into the euphotic zone initiates a phytoplankton
 1593 bloom. We see evidence of early upwelling at coastal stations where nitrate concentrations at the chlorophyll
 1594 maximum are not completely depleted (average $5.2 \pm 3.6 \mu\text{M}$), while nitrate at offshore station chlorophyll maxima are
 1595 lower (average $0.6 \pm 0.4 \mu\text{M}$). With phytoplankton growth fueled by new nitrate, the ammonium concentration begins
 1596 to increase via degradation and grazing, providing substrate for ammonia oxidizers. Rate measurements show a small

1606 increase in average ammonia oxidation rate at coastal stations compared to offshore stations (25.8 ± 3.6 vs. 21.3 ± 3.3
1607 nM day $^{-1}$, respectively). At some coastal stations, a more significant change in the concentration of the nitrite
1608 maximum may come from increased phytoplankton nitrite release. Previous work has documented up to ~10% of
1609 nitrate uptake can be released as nitrite in laboratory culture experiments, suggesting that locations with high nitrate
1610 uptake and active nitrate reduction have the potential for substantial nitrite release from phytoplankton (Collos, 1998).
1611 Additionally, the physical upwelling of deep water compresses density layers in the euphotic zone leading to higher
1612 Brunt-Väisälä frequencies and lower potential for nitrite diffusion away from the site of production, helping to explain
1613 larger nitrite maxima occurring at upwelling sites.

Deleted: Nitrate reduction rates larger than ammonia oxidation rates (>30 nM day $^{-1}$) were measured sporadically at stations near the coast.

Deleted: more

Deleted: values

1614 With nitrite production in the PNM predominantly linked to ammonia oxidation, this has potential implications for
1615 production of nitrous oxide in the upper water column of the ETNP. The ETNP is known to be an important source
1616 for atmospheric nitrous oxide (Babbin et al., 2020; Tian et al., 2020), with high accumulations of nitrous oxide in the
1617 near surface (Kelly et al., 2021; Montreal et al., 2022). Nitrous oxide production in the near-surface maximum has been
1618 linked to a combination of hybrid production from AOA, and bacterial denitrification (Kelly et al., 2021; Montreal et
1619 al., 2022; Trimmer et al., 2016). Thus, conditions that favor enhanced ammonia oxidation could also promote enhanced
1620 nitrous oxide production and emissions, thereby forming a link between stimulation of high primary productivity and
1621 high rates of nitrous oxide production and emission.

Moved (insertion) [10]

1622 5 Conclusions

1623 This study used both high resolution environmental data and direct rate measurements of nitrite cycling processes to
1624 explore the factors contributing to PNM formation in ETNP. At our sites, there was a distinct and predictable depth
1625 where nitrite accumulated in a peak-shaped PNM feature. Linear regression and multivariate regression analysis with
1626 environmental data showed that the top of the nitracline and the top of the oxycline are two major indicators of the
1627 depth of the nitrite maximum. Rate measurements also showed distinct peaks in activity that corresponded well with
1628 the mean PNM isopycnal for the region. Ammonia oxidation was the dominant nitrite production process at most
1629 depths and stations, and nitrifier processes dominated nitrite cycling at and below the PNM. Phytoplankton processes
1630 were typically restricted to depths above the PNM, and we report only a handful of high nitrate reduction rates (>20
1631 nM day $^{-1}$) from coastal stations with higher chlorophyll and nitrate concentrations at the PNM. However, even where
1632 nitrite production from phytoplankton remains low, we suggest a sequential and competitive dependence of ammonia
1633 oxidation rates on phytoplankton processes. The importance of co-occurring environmental conditions and timing of
1634 microbial interactions should be considered in further work on what factors determine the formation of large nitrite
1635 maxima. For example, both nitrate and light availability may work together to control net nitrite production through
1636 sequential processes beginning with upwelling events. Microbial physiological responses remain important in
1637 connecting rates of activity to dynamic environmental conditions.

Deleted: data

Deleted: Nitrifier

Deleted: , while phytoplankton

Deleted: . Ammonia oxidation was the dominant nitrite production process at most depths and stations. We

Deleted: , which suggest there are opportunities for phytoplankton to play a larger role in nitrite production at the PNM under these conditions.

Deleted: lag

Deleted: determines

Deleted:

1654 **References**

- 1655 Al-Qutob, M., Häse, C., Tilzer, M. M., and Lazar, B.: Phytoplankton drives nitrite dynamics in the Gulf of Aqaba,
1656 Red Sea, 239, 233–239, <https://doi.org/10.3354/meps239233>, 2002.
- 1657 Babbin, A. R., Boles, E. L., Mühlé, J., and Weiss, R. F.: On the natural spatio-temporal heterogeneity of South Pacific
1658 nitrous oxide, 11, 1–9, <https://doi.org/10.1038/s41467-020-17509-6>, 2020.
- 1659 Beman, J. M., Popp, B. N., and Francis, C. A.: Molecular and biogeochemical evidence for ammonia oxidation by
1660 marine Crenarchaeota in the Gulf of California, 2, 429–441, <https://doi.org/10.1038/ismej.2007.118>, 2008.
- 1661 Beman, J. M., Popp, B. N., and Alford, S. E.: Quantification of ammonia oxidation rates and ammonia-oxidizing
1662 archaea and bacteria at high resolution in the Gulf of California and eastern tropical North Pacific Ocean, 57, 711–
1663 726, <https://doi.org/10.4319/lo.2012.57.3.0711>, 2012.
- 1664 Beman, J. M., Shih, J. L., and Popp, B. N.: Nitrite oxidation in the upper water column and oxygen minimum zone of
1665 the eastern tropical North Pacific Ocean, 7, 2192–2205, <https://doi.org/10.1038/ismej.2013.96>, 2013.
- 1666 Böhlke, J. K., Mroczkowski, S. J., and Coplen, T. B.: Oxygen isotopes in nitrate: new reference materials for ^{18}O : ^{17}O : ^{16}O
1667 measurements and observations on nitrate-water equilibration: Reference materials for O-isotopes in nitrate,
1668 *Rapid Commun. Mass Spectrom.*, 17, 1835–1846, <https://doi.org/10.1002/rcm.1123>, 2003.
- 1669 Brandhorst, W.: Nitrite Accumulation in the North-East Tropical Pacific, *Nature*, 182, 679–679,
1670 <https://doi.org/10.1038/182679a0>, 1958.
- 1671 Bronk, D. A., Glibert, P. M., and Ward, B. B.: Nitrogen Uptake, Dissolved Organic Nitrogen Release, and New
1672 Production, *Science*, 265, 1843–1846, <https://doi.org/10.1126/science.265.5180.1843>, 1994.
- 1673 Buchwald, C. and Casciotti, K. L.: Isotopic ratios of nitrite as tracers of the sources and age of oceanic nitrite, 6, 308–
1674 313, <https://doi.org/10.1038/NGEO1745>, 2013.
- 1675 Burlacot, A., Richaud, P., Gosset, A., Li-Beisson, Y., and Peltier, G.: Algal photosynthesis converts nitric oxide into
1676 nitrous oxide, *Proc Natl Acad Sci USA*, 117, 2704–2709, <https://doi.org/10.1073/pnas.1915276117>, 2020.
- 1677 Carlucci, A. F., Hartwig, E. O., and Bowes, P. M.: Biological production of nitrite in seawater, 7, 161–166,
1678 <https://doi.org/10.1007/BF00354921>, 1970.
- 1679 Casciotti, K. L., Böhlke, J. K., McIlvin, M. R., Mroczkowski, S. J., and Hannon, J. E.: Oxygen isotopes in nitrite:
1680 analysis, calibration, and equilibration, 79, 2427–2436, <https://doi.org/10.1021/ac061598h>, 2007.
- 1681 Cline, J. D. and Richards, F. A.: Oxygen deficient conditions and nitrate reduction in the eastern tropical North Pacific
1682 Ocean, 17, 885–900, <https://doi.org/10.4319/lo.1972.17.6.0885>, 1972.
- 1683 Codispoti, L. A., Friederich, G. E., Murray, J. W., and Sakamoto, C. M.: Chemical variability in the Black Sea:
1684 implications of continuous vertical profiles that penetrated the oxic/anoxic interface, *Deep Sea Research Part A*.
1685 *Oceanographic Research Papers*, 38, S691–S710, [https://doi.org/10.1016/S0198-0149\(10\)80004-4](https://doi.org/10.1016/S0198-0149(10)80004-4), 1991.
- 1686 Collos, Y.: Transient situations in nitrate assimilation by marine diatoms. 2. Changes in nitrate and nitrite following a
1687 nitrate perturbation, 27, 528–535, <https://doi.org/10.1.1.597.3625>, 1982.
- 1688 Collos, Y.: Nitrate uptake, nitrite release and uptake, and new production estimates, 171, 293–301, 1998.
- 1689 Corne, M., Claustre, H., Mignot, A., Guidi, L., Lacour, L., Poteau, A., D'Ortenzio, F., Gentili, B., and Schmechtig,
1690 C.: Deep Chlorophyll Maxima in the Global Ocean: Occurrences, Drivers and Characteristics, *Global Biogeochem*
1691 *Cycles*, 35, <https://doi.org/10.1029/2020GB006759>, 2021.

Moved up [10]: With nitrite production in the PNM predominantly linked to ammonia oxidation, this has potential implications for production of nitrous oxide in the upper water column of the ETNP. The ETNP is known to be an important source for atmospheric nitrous oxide (Babbin et al., 2020; Tian et al., 2020), with high accumulations of nitrous oxide in the near surface (Kelly et al., 2021; Monreal et al., 2022). Nitrous oxide production in the near-surface maximum has been linked to a combination of hybrid production from AOA, and bacterial denitrification (Kelly et al., 2021; Monreal et al., 2022; Trimmer et al., 2016).

Deleted: Conditions that favor enhanced ammonia oxidation could thus also promote enhanced nitrous oxide production and emissions thereby forming a link between stimulation of high primary productivity and high rates of nitrous oxide production and emission. 

- 1708 Dore, J. E. and Karl, D. M.: Nitrification in the euphotic zone as a source for nitrite, nitrate, and nitrous oxide at Station
1709 ALOHA, 41, 1619–1628, <https://doi.org/10.4319/lo.1996.41.8.1619>, 1996.
- 1710 Dugdale, R. and Goering, J.: Uptake of new and regenerated forms of nitrogen in primary productivity, 12, 196–206,
1711 1967.
- 1712 Dugdale, R. and Wilkerson, F.: The use of ^{15}N to measure nitrogen uptake in eutrophic oceans; experimental
1713 considerations1, 2, 31, 673–689, 1986.
- 1714 Eppley, R. W. and Coatsworth, J. L.: Uptake of nitrate and nitrite by Ditylum Brightwelli - Kinetics and mechanisms,
1715 4, 151–156, <https://doi.org/10.1111/j.1529-8817.1968.tb04689.x>, 1968.
- 1716 Francis, C. A., Roberts, K. J., Beman, J. M., Santoro, A. E., and Oakley, B. B.: Ubiquity and diversity of
1717 ammoniaoxidizing archaea in water columns and sediments of the ocean, 102, 14683–14688,
1718 <https://doi.org/10.1073/pnas.0506625102>, 2005.
- 1719 Francis, C. A., Beman, J. M., and Kuypers, M. M. M.: New processes and players in the nitrogen cycle: the
1720 microbial ecology of anaerobic and archaeal ammonia oxidation, 1, 19–27, <https://doi.org/10.1038/ismej.2007.8>,
1721 2007.
- 1722 French, D. P., Furnas, M. J., and Smayda, T. J.: Diel changes in nitrite concentration in the chlorophyll maximum in
1723 the Gulf of Mexico, 30, 707–722, <https://doi.org/10.1073/pnas.0506625102>, 1983.
- 1724 Füssel, J., Lam, P., Lavik, G., Jensen, M. M., Holtappels, M., Günter, M., and Kuypers, M. M.: Nitrite oxidation in
1725 the Namibian oxygen minimum zone, 6, 1200–1209, <https://doi.org/10.1038/ismej.2011.178>, 2012.
- 1726 Glibert, P. M., Middelburg, J. J., McClelland, J. W., and Jake Vander Zanden, M.: Stable isotope tracers: Enriching
1727 our perspectives and questions on sources, fates, rates, and pathways of major elements in aquatic systems, Limnol
1728 Oceanogr, 64, 950–981, <https://doi.org/10.1002/limo.11087>, 2019.
- 1729 GLODAP, V.: GLODAP V2, V2.
- 1730 Granger, J. and Sigman, D. M.: Removal of nitrite with sulfamic acid for nitrate N and O isotope analysis with the
1731 denitrifier method, 23, 3753–3762, <https://doi.org/10.1002/rcm.4307>, 2009.
- 1732 Grömping, U.: Relative Importance for Linear Regression in R: The Package relaimpo, 17, 1–27, 2006.
- 1733 Gruber, N.: The marine nitrogen cycle: overview and challenges, 2, 1–50, <https://doi.org/10.1038/nature06592>, 2008.
- 1734 Guerrero, M. A. and Jones, R. D.: Photoinhibition of marine nitrifying bacteria. I. Wavelength-dependent response,
1735 141, 183–192, <https://doi.org/10.3354/meps141183>, 1996.
- 1736 Herland, A. and Voituriez, B.: Hydrological structure analysis for estimating the primary production in the tropical
1737 Atlantic Ocean, 37, 16, 1979.
- 1738 Holligan, P. M., Balch, W. M., and Yentsch, C. M.: The significance of subsurface chlorophyll, nitrite and
1739 ammonium maxima in relation to nitrogen for phytoplankton growth in stratified waters of the Gulf of Maine, 42,
1740 1051–1073, <https://doi.org/10.1357/00224084788520747>, 1984.
- 1741 Holmes, R. M., Aminot, A., Kéroutel, R., Hooker, B. A., and Peterson, B. J.: A simple and precise method for
1742 measuring ammonium in marine and freshwater ecosystems, 56, 1801–1808, <https://doi.org/10.1139/f99-128>, 1999.
- 1743 Horak, R. E. A., Qin, W., Bertagnolli, A. D., Nelson, A., Heal, K. R., Han, H., Heller, M., Schauer, A. J., Jeffrey, W.
1744 H., Armbrust, E. V., Moffett, J. W., Ingalls, A. E., Stahl, D. A., and Devol, A. H.: Relative impacts of light,

- 1745 temperature, and reactive oxygen on thaumarchaeal ammonia oxidation in the North Pacific Ocean, 63, 741–757,
1746 <https://doi.org/10.1002/lno.10665>, 2018.
- 1747 Kelly, C. L., Travis, N. M., Baya, P. A., and Casciotti, K. L.: Quantifying Nitrous Oxide Cycling Regimes in the
1748 Eastern Tropical North Pacific Ocean With Isotopomer Analysis, Global Biogeochem Cycles, 35,
1749 <https://doi.org/10.1029/2020GB006637>, 2021.
- 1750 Kiefer, D., Olson, R., and Holm-Hansen, O.: Another look at the nitrite and chlorophyll maxima in the central North
1751 Pacific, in: Deep Sea Research and Oceanographic Abstracts, 1199–1208,
1752 [https://doi.org/10.1016/00117471\(76\)90895-0](https://doi.org/10.1016/00117471(76)90895-0), 1976.
- 1753 Legendre-Fixx, M.: Drivers of phytoplankton community heterogeneity in the Eastern Tropical North Pacific,
1754 Undergraduate Thesis, University of Washington, 2017.
- 1755 Lomas, M. and Glibert, P.: Interactions between NH₄⁺ and NO₃⁻ uptake and assimilation: comparison of diatoms
1756 and dinoflagellates at several growth temperatures, 133, 541–551, <https://doi.org/10.1007/s002270050494>, 1999.
- 1757 Lomas, M. W. and Glibert, P. M.: Comparisons of nitrate uptake, storage, and reduction in marine diatoms and
1758 flagellates, 36, 903–913, <https://doi.org/10.1046/j.1529-8817.2000.99029.x>, 2000.
- 1759 Lomas, M. W. and Lipschultz, F.: Forming the primary nitrite maximum: Nitrifiers or phytoplankton?, 51, 2453–2467,
1760 <https://doi.org/10.4319/lo.2006.51.5.2453>, 2006.
- 1761 Lücker, S., Wagner, M., Maixner, F., Pelletier, E., Koch, H., Vacherie, B., Rattei, T., Damsté, J. S. S., Speck, E., Le
1762 Paslier, D., and Daims, H.: A *Nitrosira* metagenome illuminates the physiology and evolution of globally important
1763 nitrite-oxidizing bacteria, Proc. Natl. Acad. Sci. U.S.A., 107, 13479–13484,
1764 <https://doi.org/10.1073/pnas.1003860107>, 2010.
- 1765 Lücker, S., Nowka, B., Rattei, T., Speck, E., and Daims, H.: The Genome of Nitrospina gracilis Illuminates the
1766 Metabolism and Evolution of the Major Marine Nitrite Oxidizer, Front. Microbiol., 4,
1767 <https://doi.org/10.3389/fmicb.2013.00027>, 2013.
- 1768 Mackey, K. R., Bristow, L., Parks, D. R., Altabet, M. A., Post, A. F., and Paytan, A.: The influence of light on
1769 nitrogen cycling and the primary nitrite maximum in a seasonally stratified sea, 91, 545–560,
1770 <https://doi.org/10.1016/j.pocean.2011.09.001>, 2011.
- 1771 Martens-Habbena, W., Berube, P. M., Urakawa, H., de la Torre, J. R., and Stahl, D. A.: Ammonia oxidation kinetics
1772 determine niche separation of nitrifying Archaea and Bacteria, Nature, 461, 976–979,
1773 <https://doi.org/10.1038/nature08465>, 2009.
- 1774 McIlvin, M. R. and Altabet, M. A.: Chemical conversion of nitrate and nitrite to nitrous oxide for nitrogen and oxygen
1775 isotopic analysis in freshwater and seawater, 77, 5589–5595, <https://doi.org/10.1021/ac050528s>, 2005.
- 1776 McIlvin, M. R. and Casciotti, K. L.: Technical updates to the bacterial method for nitrate isotopic analyses, 83, 1850–
1777 1856, <https://doi.org/10.1021/ac1028984>, 2011.
- 1778 Meeder, E., Mackey, K. R., Paytan, A., Shaked, Y., Iluz, D., Stambler, N., Rivlin, T., Post, A. F., and Lazar, B.:
1779 Nitrite dynamics in the open ocean—clues from seasonal and diurnal variations, 453,
1780 <https://doi.org/10.3354/meps09525>, 2012.
- 1781 Merbt, S. N., Stahl, D. A., Casamayor, E. O., Martí, E., Nicol, G. W., and Prosser, J. I.: Differential photoinhibition
1782 of bacterial and archaeal ammonia oxidation, 327, 41–46, <https://doi.org/10.1111/j.1574-6968.2011.02457.x>, 2012.
- 1783 Miller, T. L. based on F. code by A.: leaps: Regression Subset Selection, 2020.

- 1784 Miller, J. and Miller, J.: *Statistics for Analytical Chemistry*, 2nd, Ed., John Wiley & Sons, NY, 1988.
- 1785 Mincer, T. J., Church, M. J., Taylor, L. T., Preston, C., Karl, D. M., and DeLong, E. F.: Quantitative distribution of
1786 presumptive archaeal and bacterial nitrifiers in Monterey Bay and the North Pacific Subtropical Gyre, 9, 1162–1175,
1787 https://doi.org/10.1111/j.1462-2920.2007.01239.x, 2007.
- 1788 Monreal, P. J., Kelly, C. L., Travis, N. M., and Casciotti, K. L.: Identifying the Sources and Drivers of Nitrous
1789 Oxide Accumulation in the Eddy-Influenced Eastern Tropical North Pacific Oxygen-Deficient Zone, *Global
1790 Biogeochemical Cycles*, 36, https://doi.org/10.1029/2022GB007310, 2022.
- 1791 Mulholland, M. R. and Lomas, M. W.: Nitrogen uptake and assimilation, 303–384, 2008.
- 1792 Olson, R. J.: Differential photoinhibition of marine nitrifying bacteria: a possible mechanism for the formation of the
1793 primary nitrite maximum, 39, 227–238, 1981.
- 1794 Peng, X., Fuchsman, C. A., Jayakumar, A., Oleynik, S., Martens-Habbena, W., Devol, A. H., and Ward, B. B.:
1795 Ammonia and nitrite oxidation in the Eastern Tropical North Pacific: AMMONIA AND NITRITE OXIDATION IN
1796 ETNP, 29, 2034–2049, https://doi.org/10.1002/2015GB005278, 2015.
- 1797 Plouviez, M., Shilton, A., Packer, M. A., and Guiyesse, B.: Nitrous oxide emissions from microalgae: potential
1798 pathways and significance, *J Appl Phycol*, 31, 1–8, https://doi.org/10.1007/s10811-018-1531-1, 2019.
- 1799 Raimbault, P.: Effect of temperature on nitrite excretion by three marine diatoms during nitrate uptake, 92, 149–155,
1800 1986.
- 1801 Rajaković, L. V., Marković, D. D., Rajaković-Ognjanović, V. N., and Antanasićević, D. Z.: The approaches for
1802 estimation of limit of detection for ICP-MS trace analysis of arsenic, *Talanta*, 102, 79–87, 2012.
- 1803 Sakamoto, C. M., Friederich, G. E., and Codispoti, L. A.: MBARI procedures for automated nutrient analyses using a
1804 modified Alpkem Series 300 Rapid Flow Analyzer, 1990.
- 1805 Santoro, A., Sakamoto, C., Smith, J., Plant, J., Gehman, A., Worden, A., Johnson, K., Francis, C., and Casciotti, K.:
1806 Measurements of nitrite production in and around the primary nitrite maximum in the central California Current, 10,
1807 7395–7410, 2013.
- 1808 Santoro, A. E., Casciotti, K. L., and Francis, C. A.: Activity, abundance and diversity of nitrifying archaea and bacteria
1809 in the central California Current, 12, 1989–2006, 2010.
- 1810 Santoro, A. E., Buchwald, C., McIlvin, M. R., and Casciotti, K. L.: Isotopic signature of N₂O produced by marine
1811 ammonia-oxidizing archaea, 333, 1282–1285, 2011.
- 1812 Schaefer, S. C. and Hollibaugh, J. T.: Temperature Decouples Ammonium and Nitrite Oxidation in Coastal Waters,
1813 51, 3157–3164, https://doi.org/10.1021/acs.est.6b03483, 2017.
- 1814 Schleper, C., Jurgens, G., and Jonuscheit, M.: Genomic studies of uncultivated archaea, *Nat Rev Microbiol*, 3, 479–
1815 488, https://doi.org/10.1038/nrmicro1159, 2005.
- 1816 Shiozaki, T., Ijichi, M., Isobe, K., Hashihama, F., Nakamura, K., Ehama, M., Hayashizaki, K., Takahashi, K.,
1817 Hamasaki, K., and Furuya, K.: Nitrification and its influence on biogeochemical cycles from the equatorial Pacific
1818 to the Arctic Ocean, 10, 2184, 2016.
- 1819 Sigman, D. M., Casciotti, K. L., Andreani, M., Barford, C., Galanter, M., and Böhlke, J. K.: A Bacterial Method for
1820 the Nitrogen Isotopic Analysis of Nitrate in Seawater and Freshwater, *Anal. Chem.*, 73, 4145–4153,
1821 https://doi.org/10.1021/ac010088e, 2001.

Formatted: Font: (Default) Times New Roman, 10 pt

Formatted: Line spacing: single

Deleted: ¶

- 1823 Smith, J. M., Chavez, F. P., and Francis, C. A.: Ammonium uptake by phytoplankton regulates nitrification in the
1824 sunlit ocean, 9, e108173, 2014.
- 1825 Strickland, J. D. and Parsons, T. R.: A practical handbook of seawater analysis, 1972.
- 1826 Tian, H., Xu, R., Canadell, J. G., Thompson, R. L., Winiwarter, W., Suntharalingam, P., Davidson, E. A., Ciais, P.,
1827 Jackson, R. B., Janssens-Maenhout, G., Prather, M. J., Regnier, P., Pan, N., Pan, S., Peters, G. P., Shi, H., Tubiello,
1828 F. N., Zaeble, S., Zhou, F., Arneth, A., Battaglia, G., Berthet, S., Bopp, L., Bouwman, A. F., Buitenhuis, E. T.,
1829 Chang, J., Chipperfield, M. P., Dangal, S. R. S., Dlugokencky, E., Elkins, J. W., Eyre, B. D., Fu, B., Hall, B., Ito, A.,
1830 Joos, F., Krummel, P. B., Landolfi, A., Laruelle, G. G., Lauerwald, R., Li, W., Lienert, S., Maavara, T., MacLeod,
1831 M., Millet, D. B., Olin, S., Patra, P. K., Prinn, R. G., Raymond, P. A., Ruiz, D. J., van der Werf, G. R., Vuichard, N.,
1832 Wang, J., Weiss, R. F., Wells, K. C., Wilson, C., Yang, J., and Yao, Y.: A comprehensive quantification of global
1833 nitrous oxide sources and sinks, *Nature*, 586, 248–256, <https://doi.org/10.1038/s41586-020-2780-0>, 2020.
- 1834 Trimmer, M., Chronopoulou, P.-M., Maanoja, S. T., Upstill-Goddard, R. C., Kitidis, V., and Purdy, K. J.: Nitrous
1835 oxide as a function of oxygen and archaeal gene abundance in the North Pacific, *Nat Commun*, 7, 13451,
1836 <https://doi.org/10.1038/ncomms13451>, 2016.
- 1837 Vaccaro, R. F. and Ryther, J. H.: Marine Phytoplankton and the Distribution of Nitrite in the Sea*, 25, 260–271,
1838 <https://doi.org/10.1093/icesjms/25.3.260>, 1960.
- 1839 Wada, E. and Hattori, A.: Nitrite metabolism in the euphotic layer of the central North Pacific Ocean, 16, 766–772,
1840 1971.
- 1841 Wada, E. and Hattori, A.: Nitrite distribution and nitrate reduction in deep sea waters, 19, 123–132,
1842 [https://doi.org/10.1016/0011-7471\(72\)90044-7](https://doi.org/10.1016/0011-7471(72)90044-7), 1972.
- 1843 Wan, X. S., Sheng, H.-X., Dai, M., Zhang, Y., Shi, D., Trull, T. W., Zhu, Y., Lomas, M. W., and Kao, S.-J.:
1844 Ambient nitrate switches the ammonium consumption pathway in the euphotic ocean, *Nat Commun*, 9, 915,
1845 <https://doi.org/10.1038/s41467-018-03363-0>, 2018.
- 1846 Wan, X. S., Sheng, H., Dai, M., Church, M. J., Zou, W., Li, X., Hutchins, D. A., Ward, B. B., and Kao, S.:
1847 Phytoplankton-nitrifier interactions control the geographic distribution of nitrite in the upper ocean, *Global
1848 Biogeochem Cycles*, <https://doi.org/10.1029/2021GB007072>, 2021.
- 1849 Ward, B. and Carlucci, A.: Marine ammonia-and nitrite-oxidizing bacteria: serological diversity determined by
1850 immunofluorescence in culture and in the environment, 50, 194–201, <https://doi.org/10.1128/aem.50.2.194201.1985>,
1851 1985.
- 1852 Ward, B. B.: Light and substrate concentration relationships with marine ammonium assimilation and oxidation rates,
1853 16, 301–316, [https://doi.org/10.1016/0304-4203\(85\)90052-0](https://doi.org/10.1016/0304-4203(85)90052-0), 1985.
- 1854 Ward, B. B.: Temporal variability in nitrification rates and related biogeochemical factors in Monterey Bay, California,
1855 USA, *Mar Ecol Prog Ser*, 292, 97–109, <https://doi.org/10.3354/meps292097>, 2005.
- 1856 Ward, B. B., Olson, R. J., and Perry, M. J.: Microbial nitrification rates in the primary nitrite maximum off southern
1857 California, 29, 247–255, [https://doi.org/10.1016/0198-0149\(82\)90112-1](https://doi.org/10.1016/0198-0149(82)90112-1), 1982.
- 1858 Ward, B. B., Kilpatrick, K. A., Renger, E. H., and Eppley, R. W.: Biological nitrogen cycling in the nitracline, 34,
1859 493–513, <https://doi.org/10.4319/lo.1989.34.3.0493>, 1989.
- 1860 Watson, S. W. and Waterbury, J. B.: Characteristics of two marine nitrite oxidizing bacteria, *Nitrospina gracilis* nov.
1861 gen. nov. sp. and *Nitrococcus mobilis* nov. gen. nov. sp., 77, 203–230, 1971.

- 1862 Xu, M. N., Li, X., Shi, D., Zhang, Y., Dai, M., Huang, T., Glibert, P. M., and Kao, S.: Coupled effect of substrate
1863 and light on assimilation and oxidation of regenerated nitrogen in the euphotic ocean, *Limnol Oceanogr*, 64, 1270–
1864 1283, <https://doi.org/10.1002/lno.11114>, 2019.
- 1865 Yool, A., Martin, A. P., Fernández, C., and Clark, D. R.: The significance of nitrification for oceanic new production,
1866 447, 999–1002, <https://doi.org/10.1038/nature05885>, 2007.
- 1867 Zafiriou, O. C., Ball, L. A., and Hanley, Q.: Trace nitrate in oxic waters, 39, 1329–1347, [https://doi.org/10.1016/0198-0149\(92\)90072-2](https://doi.org/10.1016/0198-0149(92)90072-2), 1992.
- 1869 Zakem, E. J., Al-Haj, A., Church, M. J., van Dijken, G. L., Dutkiewicz, S., Foster, S. Q., Fulweiler, R. W., Mills, M.
1870 M., and Follows, M. J.: Ecological control of nitrite in the upper ocean, 9, <https://doi.org/10.1038/s41467-01803553-w>, 2018.
- 1872 Zehr, J. P. and Kudela, R. M.: Nitrogen Cycle of the Open Ocean: From Genes to Ecosystems, *Annu. Rev. Mar. Sci.*,
1873 3, 197–225, <https://doi.org/10.1146/annurev-marine-120709-142819>, 2011.
- 1874 Zehr, J. P. and Ward, B. B.: Nitrogen Cycling in the Ocean: New Perspectives on Processes and Paradigms, *AEM*, 68,
1875 1015–1024, <https://doi.org/10.1128/AEM.68.3.1015-1024.2002>, 2002.

1876
1877 **Acknowledgements**

1878 The authors acknowledge the captain and crew of the research vessels required to collect this data set:
1879 R/V Ronald Brown, R/V Sikuliaq, R/V Sally Ride and the R/V Falkor. We also acknowledge shipboard
1880 support from Marguerite Blum and Matt Forbes. This research was supported by U.S.-NSF grant
1881 OCE1657868 to K. L. Casciotti.

1882

1883 **Author Contributions**

1884 Major data collection efforts, data processing/analysis and writing were conducted by N. Travis.
1885 Significant support during data collection was provided by C. Kelly and M. Mulholland, with additional
1886 contributions during manuscript editing. K. Casciotti was instrumental in initial project design, laboratory
1887 analysis, data investigations and manuscript writing.

Page 6: [1] Formatted Nicole Travis 10/13/22 2:31:00 PM

Font: 10 pt, Subscript

Page 6: [1] Formatted Nicole Travis 10/13/22 2:31:00 PM

Font: 10 pt, Subscript

Page 6: [2] Formatted Nicole Travis 10/13/22 2:31:00 PM

Font: 10 pt, Subscript

Page 6: [2] Formatted Nicole Travis 10/13/22 2:31:00 PM

Font: 10 pt, Subscript

Page 6: [3] Formatted Nicole Travis 10/13/22 2:31:00 PM

Font: 10 pt, Subscript

Page 6: [3] Formatted Nicole Travis 10/13/22 2:31:00 PM

Font: 10 pt, Subscript

Page 6: [4] Formatted Nicole Travis 10/13/22 2:31:00 PM

Font: 10 pt, Subscript

Page 6: [4] Formatted Nicole Travis 10/13/22 2:31:00 PM

Font: 10 pt, Subscript

Page 6: [5] Formatted Nicole Travis 10/13/22 2:31:00 PM

Font: 10 pt, Subscript

Page 6: [5] Formatted Nicole Travis 10/13/22 2:31:00 PM

Font: 10 pt, Subscript

Page 6: [6] Formatted Nicole Travis 10/13/22 2:31:00 PM

Font: 10 pt, Subscript

Page 6: [6] Formatted Nicole Travis 10/13/22 2:31:00 PM

Font: 10 pt, Subscript

Page 6: [7] Formatted Nicole Travis 10/13/22 2:31:00 PM

Font: 10 pt, Subscript

Page 6: [7] Formatted Nicole Travis 10/13/22 2:31:00 PM

Font: 10 pt, Subscript

Page 6: [8] Formatted Nicole Travis 10/13/22 2:31:00 PM

Font: 10 pt, Subscript

Page 6: [8] Formatted Nicole Travis 10/13/22 2:31:00 PM

Font: 10 pt, Subscript

Page 6: [9] Deleted Nicole Travis 10/13/22 2:31:00 PM

Page 6: [9] Deleted Nicole Travis 10/13/22 2:31:00 PM

Page 6: [10] Deleted Nicole Travis 10/13/22 2:31:00 PM

Page 6: [10] Deleted Nicole Travis 10/13/22 2:31:00 PM

Page 6: [10] Deleted Nicole Travis 10/13/22 2:31:00 PM

Page 8: [11] Deleted Nicole Travis 10/13/22 2:31:00 PM

Page 8: [11] Deleted Nicole Travis 10/13/22 2:31:00 PM

Page 8: [11] Deleted Nicole Travis 10/13/22 2:31:00 PM

Page 8: [11] Deleted Nicole Travis 10/13/22 2:31:00 PM

Page 8: [11] Deleted Nicole Travis 10/13/22 2:31:00 PM

Page 8: [12] Formatted Nicole Travis 10/13/22 2:31:00 PM

Font: 10 pt

Page 8: [13] Deleted Nicole Travis 10/13/22 2:31:00 PM

Page 8: [14] Formatted Nicole Travis 10/13/22 2:31:00 PM

Font: 10 pt

Page 8: [15] Formatted Nicole Travis 10/15/22 11:29:00 PM

Font: Times New Roman, No underline, Underline color: Auto

Page 8: [16] Formatted Nicole Travis 10/15/22 11:30:00 PM

Centered

Page 8: [17] Formatted Table Nicole Travis 10/15/22 11:30:00 PM

Formatted Table

Page 8: [18] Formatted Nicole Travis 10/15/22 11:30:00 PM

Centered, Indent: Left: 0", First line: 0"

Page 8: [19] Formatted Nicole Travis 10/15/22 11:29:00 PM

Font: Times New Roman, No underline, Underline color: Auto

Page 8: [20] Formatted Nicole Travis 10/15/22 11:29:00 PM

Font: Times New Roman, No underline, Underline color: Auto

Page 8: [21] Formatted Nicole Travis 10/15/22 11:30:00 PM

Centered, Indent: Left: 0"

Page 8: [22] Formatted Nicole Travis 10/15/22 11:29:00 PM

Font: Times New Roman, No underline, Underline color: Auto

Page 8: [23] Formatted Nicole Travis 10/15/22 11:30:00 PM

Centered, Indent: Left: 0", First line: 0"

Page 8: [24] Formatted Nicole Travis 10/15/22 11:29:00 PM

Font: Times New Roman, No underline, Underline color: Auto

Page 8: [24] Formatted Nicole Travis 10/15/22 11:29:00 PM

Font: Times New Roman, No underline, Underline color: Auto

Page 8: [25] Formatted Nicole Travis 10/15/22 11:29:00 PM

Font: Times New Roman

Page 8: [26] Deleted Nicole Travis 10/13/22 2:31:00 PM

Page 8: [27] Formatted Nicole Travis 10/15/22 11:29:00 PM

No underline, Underline color: Auto

Page 8: [28] Formatted Nicole Travis 10/15/22 11:30:00 PM

Centered

Page 8: [29] Formatted Nicole Travis 10/15/22 11:29:00 PM

Font: Times New Roman, No underline, Underline color: Auto

Page 8: [30] Formatted Nicole Travis 10/13/22 2:31:00 PM

Font: Times New Roman, Not Italic

Page 8: [31] Formatted Nicole Travis 10/15/22 11:29:00 PM

Justified, Line spacing: single

Page 8: [32] Formatted Nicole Travis 10/15/22 11:29:00 PM

Justified, Indent: Left: 0", Line spacing: single

Page 8: [33] Formatted Nicole Travis 10/13/22 2:31:00 PM

Font: Times New Roman

Page 8: [34] Formatted Nicole Travis 10/13/22 2:31:00 PM

Font: Times New Roman

Page 8: [35] Formatted Nicole Travis 10/13/22 2:31:00 PM

Font: Times New Roman

Page 8: [36] Formatted Nicole Travis 10/13/22 2:31:00 PM

Font: Times New Roman

Page 8: [37] Formatted Nicole Travis 10/15/22 11:29:00 PM

Justified, Right: 0", Line spacing: single

Page 8: [38] Formatted Nicole Travis 10/13/22 2:31:00 PM

Font: Times New Roman, Not Italic

Page 8: [39] Formatted Nicole Travis 10/15/22 11:29:00 PM

Justified, Line spacing: single

Page 8: [40] Formatted Nicole Travis 10/15/22 11:29:00 PM

Justified, Indent: Left: 0", Line spacing: single

Page 8: [41] Formatted Nicole Travis 10/15/22 11:29:00 PM

Justified, Indent: Left: 0", First line: 0", Line spacing: single

Page 8: [42] Formatted Nicole Travis 10/13/22 2:31:00 PM

Font: Times New Roman

Page 8: [43] Formatted Nicole Travis 10/13/22 2:31:00 PM

Font: Times New Roman

Page 8: [44] Formatted Nicole Travis 10/15/22 11:29:00 PM

Justified, Indent: Left: 0", Line spacing: single

Page 8: [45] Formatted Nicole Travis 10/13/22 2:31:00 PM

Font: Times New Roman

Page 8: [46] Formatted Nicole Travis 10/13/22 2:31:00 PM

Font: Times New Roman

Page 8: [47] Formatted Nicole Travis 10/15/22 11:29:00 PM

Justified, Right: 0", Line spacing: single

Page 8: [48] Formatted Nicole Travis 10/13/22 2:31:00 PM

Font: Times New Roman, Not Italic

Page 8: [49] Formatted Nicole Travis 10/15/22 11:29:00 PM

Justified, Line spacing: single

Page 8: [50] Formatted Nicole Travis 10/15/22 11:29:00 PM

Justified, Indent: Left: 0", Line spacing: single

Page 8: [51] Formatted Nicole Travis 10/13/22 2:31:00 PM

Font: Times New Roman

Page 8: [52] Formatted Nicole Travis 10/13/22 2:31:00 PM

Font: Times New Roman

Page 8: [53] Formatted Nicole Travis 10/13/22 2:31:00 PM

Font: Times New Roman

Page 8: [54] Formatted Nicole Travis 10/13/22 2:31:00 PM

Font: Times New Roman

Page 8: [55] Formatted Nicole Travis 10/15/22 11:29:00 PM

Justified, Right: 0", Line spacing: single

Page 8: [56] Deleted Nicole Travis 10/13/22 2:31:00 PM

Page 8: [57] Formatted Nicole Travis 10/13/22 2:31:00 PM

Indent: Left: 0", Space After: 11.85 pt, Line spacing: 1.5 lines

Page 8: [58] Formatted Nicole Travis 10/13/22 2:31:00 PM

Font: Times New Roman

Page 8: [59] Deleted Nicole Travis 10/13/22 2:31:00 PM

Page 8: [60] Formatted Nicole Travis 10/13/22 2:31:00 PM

Left, Indent: Left: 0", First line: 0", Space After: 11.85 pt

Page 8: [61] Formatted Nicole Travis 10/13/22 2:31:00 PM

Font color: Text 1

Page 8: [61] Formatted Nicole Travis 10/13/22 2:31:00 PM

Font color: Text 1

Page 8: [62] Formatted Nicole Travis 10/13/22 2:31:00 PM

Font: Times New Roman, Font color: Text 1

Page 8: [62] Formatted Nicole Travis 10/13/22 2:31:00 PM

Font: Times New Roman, Font color: Text 1

Page 8: [63] Formatted Nicole Travis 10/13/22 2:31:00 PM

Font color: Text 1

Page 8: [64] Formatted Nicole Travis 10/13/22 2:31:00 PM

Font color: Text 1

Page 8: [65] Formatted Nicole Travis 10/13/22 2:31:00 PM

Font: Times New Roman, Font color: Text 1

Page 8: [65] Formatted Nicole Travis 10/13/22 2:31:00 PM

Font: Times New Roman, Font color: Text 1

Page 8: [66] Formatted Nicole Travis 10/13/22 2:31:00 PM

Font: Times New Roman, Font color: Text 1

Page 8: [66] Formatted Nicole Travis 10/13/22 2:31:00 PM

Font: Times New Roman, Font color: Text 1

Page 8: [67] Deleted Nicole Travis 10/13/22 2:31:00 PM

Page 8: [67] Deleted Nicole Travis 10/13/22 2:31:00 PM

Page 8: [67] Deleted Nicole Travis 10/13/22 2:31:00 PM

Page 8: [68] Formatted Nicole Travis 10/13/22 2:31:00 PM

Font: Times New Roman

Page 8: [69] Deleted Nicole Travis 10/13/22 2:31:00 PM

Page 11: [70] Formatted Nicole Travis 10/13/22 2:31:00 PM

Font: Times New Roman

Page 11: [70] Formatted Nicole Travis 10/13/22 2:31:00 PM

Font: Times New Roman

Page 11: [71] Deleted Nicole Travis 10/13/22 2:31:00 PM

Page 11: [71] Deleted Nicole Travis 10/13/22 2:31:00 PM

Page 11: [72] Formatted Nicole Travis 10/13/22 2:31:00 PM

Font: Times New Roman

Page 11: [72] Formatted Nicole Travis 10/13/22 2:31:00 PM

Font: Times New Roman

Page 11: [73] Deleted Nicole Travis 10/13/22 2:31:00 PM

Page 11: [73] Deleted Nicole Travis 10/13/22 2:31:00 PM

Page 11: [73] Deleted Nicole Travis 10/13/22 2:31:00 PM

Page 11: [73] Deleted Nicole Travis 10/13/22 2:31:00 PM

Page 11: [73] Deleted Nicole Travis 10/13/22 2:31:00 PM

Page 11: [74] Deleted Nicole Travis 10/13/22 2:31:00 PM

Page 11: [75] Deleted Nicole Travis 10/13/22 2:31:00 PM

▼

▲

Page 11: [75] Deleted Nicole Travis 10/13/22 2:31:00 PM

▼

▲

Page 11: [75] Deleted Nicole Travis 10/13/22 2:31:00 PM

▼

▲

Page 11: [76] Deleted Nicole Travis 10/13/22 2:31:00 PM

▼

▲

Page 11: [76] Deleted Nicole Travis 10/13/22 2:31:00 PM

▼

▲

Page 11: [76] Deleted Nicole Travis 10/13/22 2:31:00 PM

▼

▲

Page 11: [77] Formatted Nicole Travis 10/13/22 2:31:00 PM

Indent: Left: -0.01", Hanging: 0.01", Space After: 0 pt, No bullets or numbering

▲

Page 11: [78] Deleted Nicole Travis 10/13/22 2:31:00 PM

▼

▲

Page 11: [78] Deleted Nicole Travis 10/13/22 2:31:00 PM

▼

▲

Page 11: [78] Deleted Nicole Travis 10/13/22 2:31:00 PM

▼

▲

Page 14: [79] Deleted Nicole Travis 10/13/22 2:31:00 PM

Page 18: [80] Deleted Nicole Travis 10/13/22 2:31:00 PM

Page 18: [81] Deleted Nicole Travis 10/13/22 2:31:00 PM

▼

▲

Page 18: [82] Deleted Nicole Travis 10/13/22 2:31:00 PM

▼

Page 18: [83] Deleted Nicole Travis 10/13/22 2:31:00 PM

Page 18: [84] Deleted Nicole Travis 10/13/22 2:31:00 PM

Page 18: [85] Deleted Nicole Travis 10/13/22 2:31:00 PM

Page 18: [86] Deleted Nicole Travis 10/13/22 2:31:00 PM

Page 18: [87] Deleted Nicole Travis 10/13/22 2:31:00 PM

Page 18: [88] Deleted Nicole Travis 10/13/22 2:31:00 PM

Page 20: [89] Deleted Nicole Travis 10/13/22 2:31:00 PM

Page 20: [89] Deleted Nicole Travis 10/13/22 2:31:00 PM

Page 20: [89] Deleted Nicole Travis 10/13/22 2:31:00 PM

Page 20: [89] Deleted Nicole Travis 10/13/22 2:31:00 PM

Page 20: [89] Deleted Nicole Travis 10/13/22 2:31:00 PM

Page 20: [89] Deleted Nicole Travis 10/13/22 2:31:00 PM

Page 20: [89] Deleted Nicole Travis 10/13/22 2:31:00 PM

Page 20: [89] Deleted Nicole Travis 10/13/22 2:31:00 PM

Page 20: [90] Deleted Nicole Travis 10/13/22 2:31:00 PM

Page 20: [90] Deleted Nicole Travis 10/13/22 2:31:00 PM

Page 20: [90] Deleted Nicole Travis 10/13/22 2:31:00 PM

Page 20: [90] Deleted Nicole Travis 10/13/22 2:31:00 PM

▼.....▲
Page 20: [90] Deleted Nicole Travis 10/13/22 2:31:00 PM

▼.....▲
Page 20: [90] Deleted Nicole Travis 10/13/22 2:31:00 PM

▼.....▲
Page 20: [90] Deleted Nicole Travis 10/13/22 2:31:00 PM

▼.....▲
Page 20: [90] Deleted Nicole Travis 10/13/22 2:31:00 PM

▼.....▲
Page 20: [91] Deleted Nicole Travis 10/13/22 2:31:00 PM

▼.....▲
Page 20: [91] Deleted Nicole Travis 10/13/22 2:31:00 PM

▼.....▲
Page 20: [92] Deleted Nicole Travis 10/13/22 2:31:00 PM

▼.....▲
Page 20: [92] Deleted Nicole Travis 10/13/22 2:31:00 PM

▼.....▲
Page 23: [93] Deleted Nicole Travis 10/13/22 2:31:00 PM

▼.....▲
Page 23: [94] Deleted Nicole Travis 10/13/22 2:31:00 PM

Subscript
▲
Page 25: [95] Formatted Nicole Travis 10/13/22 2:31:00 PM

Subscript
▲
Page 25: [95] Formatted Nicole Travis 10/13/22 2:31:00 PM

▼.....▲
Page 25: [96] Deleted Nicole Travis 10/13/22 2:31:00 PM

▲.....
Page 25: [96] Deleted Nicole Travis 10/13/22 2:31:00 PM

▼.....
▲.....
Page 25: [96] Deleted Nicole Travis 10/13/22 2:31:00 PM

▼.....
▲.....
Page 25: [96] Deleted Nicole Travis 10/13/22 2:31:00 PM

▼.....
▲.....
Page 25: [96] Deleted Nicole Travis 10/13/22 2:31:00 PM

▼.....
▲.....
Page 25: [96] Deleted Nicole Travis 10/13/22 2:31:00 PM

▼.....
▲.....
Page 25: [96] Deleted Nicole Travis 10/13/22 2:31:00 PM

▼.....
▲.....
Page 25: [97] Deleted Nicole Travis 10/13/22 2:31:00 PM

▼.....
▲.....
Page 25: [97] Deleted Nicole Travis 10/13/22 2:31:00 PM

▼.....
▲.....
Page 25: [98] Deleted Nicole Travis 10/13/22 2:31:00 PM

▼.....
▲.....
Page 25: [98] Deleted Nicole Travis 10/13/22 2:31:00 PM

▼.....
▲.....
Page 25: [98] Deleted Nicole Travis 10/13/22 2:31:00 PM

▼.....◀
▲.....◀
Page 25: [99] Deleted Nicole Travis 10/13/22 2:31:00 PM

▼.....◀
▲.....◀
Page 25: [99] Deleted Nicole Travis 10/13/22 2:31:00 PM

▼.....◀
▲.....◀
Page 25: [100] Deleted Nicole Travis 10/13/22 2:31:00 PM

▼.....◀
▲.....◀
Page 25: [100] Deleted Nicole Travis 10/13/22 2:31:00 PM

▼.....◀
▲.....◀
Page 25: [100] Deleted Nicole Travis 10/13/22 2:31:00 PM

▼.....◀
▲.....◀
Page 25: [101] Formatted Nicole Travis 10/13/22 2:31:00 PM

Font: Times New Roman

▼.....◀
▲.....◀
Page 25: [101] Formatted Nicole Travis 10/13/22 2:31:00 PM

Font: Times New Roman

▼.....◀
▲.....◀
Page 27: [102] Deleted Nicole Travis 10/13/22 2:31:00 PM

▼.....◀
▲.....◀
Page 27: [102] Deleted Nicole Travis 10/13/22 2:31:00 PM

▼.....◀
▲.....◀
Page 27: [102] Deleted Nicole Travis 10/13/22 2:31:00 PM

▼.....◀
▲.....◀
Page 27: [102] Deleted Nicole Travis 10/13/22 2:31:00 PM

▼.....◀
▲.....◀
Page 27: [103] Deleted Nicole Travis 10/13/22 2:31:00 PM

Page 27: [103] Deleted Nicole Travis 10/13/22 2:31:00 PM

▼

▲

Page 27: [104] Deleted Nicole Travis 10/13/22 2:31:00 PM

▼

▲

Page 27: [104] Deleted Nicole Travis 10/13/22 2:31:00 PM

▼

▲

Page 27: [104] Deleted Nicole Travis 10/13/22 2:31:00 PM

▼

▲

Page 27: [104] Deleted Nicole Travis 10/13/22 2:31:00 PM

▼

▲

Page 27: [104] Deleted Nicole Travis 10/13/22 2:31:00 PM

▼

▲

Page 27: [105] Deleted Nicole Travis 10/13/22 2:31:00 PM

▼

▲

Page 27: [105] Deleted Nicole Travis 10/13/22 2:31:00 PM

▼

▲

Page 27: [106] Deleted Nicole Travis 10/13/22 2:31:00 PM

▼

▲

Page 27: [106] Deleted Nicole Travis 10/13/22 2:31:00 PM

▼

▲

Page 27: [107] Deleted Nicole Travis 10/13/22 2:31:00 PM

▼

▲

Page 27: [107] Deleted Nicole Travis 10/13/22 2:31:00 PM

▼

▲

Page 27: [108] Deleted Nicole Travis 10/13/22 2:31:00 PM

▼

▲

Page 27: [108] Deleted Nicole Travis 10/13/22 2:31:00 PM

▼

▲

Page 27: [108] Deleted Nicole Travis 10/13/22 2:31:00 PM

▼

▲

Page 27: [108] Deleted Nicole Travis 10/13/22 2:31:00 PM

▼

▲

Page 27: [108] Deleted Nicole Travis 10/13/22 2:31:00 PM

▼

▲

Page 27: [108] Deleted Nicole Travis 10/13/22 2:31:00 PM

▼

▲

Page 27: [108] Deleted Nicole Travis 10/13/22 2:31:00 PM

▼

▲

Page 27: [108] Deleted Nicole Travis 10/13/22 2:31:00 PM

▼

▲

Page 27: [108] Deleted Nicole Travis 10/13/22 2:31:00 PM

▼

▲

Page 27: [108] Deleted Nicole Travis 10/13/22 2:31:00 PM

▼

▲

Page 27: [108] Deleted Nicole Travis 10/13/22 2:31:00 PM

▼

▲

Page 27: [108] Deleted Nicole Travis 10/13/22 2:31:00 PM

▼

▲

Page 27: [108] Deleted Nicole Travis 10/13/22 2:31:00 PM

▼

▲

Page 27: [108] Deleted Nicole Travis 10/13/22 2:31:00 PM

▼

▲

Page 27: [109] Deleted Nicole Travis 10/13/22 2:31:00 PM

▼

Page 27: [109] Deleted Nicole Travis 10/13/22 2:31:00 PM

▼

Page 27: [109] Deleted Nicole Travis 10/13/22 2:31:00 PM

▼

Page 27: [109] Deleted Nicole Travis 10/13/22 2:31:00 PM

▼